AFRL-PR-WP-TP-2005-200

FUEL CELL SUPPORT TESTING
Delivery Order 0029: Fuel Cells for Aerospace Power

Binod Kumar

SEPTEMBER 2004

Approved for public release; distribution is unlimited.

STINFO FINAL REPORT

PROPULSION DIRECTORATE
AIR FORCE MATERIEL COMMAND
AIR FORCE RESEARCH LABORATORY
WRIGHT-PATTERSON AIR FORCE BASE, OH 45433-7251

NOTICE

Using Government drawings, specifications, or other data included in this document for any purpose other than Government procurement does not in any way obligate the U.S. Government. The fact that the Government formulated or supplied the drawings, specifications, or other data does not license the holder or any other person or corporation; or convey any rights or permission to manufacture, use, or sell any patented invention that may relate to them.

This report has been reviewed and is releasable to the National Technical Information Service (NTIS). It will be available to the general public, including foreign nationals.

This technical report has been reviewed and is approved for publication.

/s/

JOSEPH P. FELLNER
Project Engineer
AFRL/PRPS

/s/

JOHN G. NARIUS
Chief
Energy Storage & Thermal Sciences Branch

/s/

BRAD BEATTY, Major, USAF
Acting Deputy Chief
Power Division

This report is published in the interest of scientific and technical information exchange and does not constitute approval or disapproval of its ideas or findings.

REPORT DOCUMENTATION PAGE

Form Approved
OMB No. 0704-0188

1. REPORT DATE *(DD-MM-YY)*	2. REPORT TYPE	3. DATES COVERED *(From - To)*
September 2004		09/26/2003 – 09/25/2004

4. TITLE AND SUBTITLE
FUEL CELL SUPPORT TESTING
Delivery Order 0029: Fuel Cells for Aerospace Power

5a. CONTRACT NUMBER
F33615-02-D-2299-0029

5b. GRANT NUMBER

5c. PROGRAM ELEMENT NUMBER
62203F

6. AUTHOR(S)
Binod Kumar

5d. PROJECT NUMBER
3145

5e. TASK NUMBER
22

5f. WORK UNIT NUMBER
9X

7. PERFORMING ORGANIZATION NAME(S) AND ADDRESS(ES)

University of Dayton Research Institute
300 College Park, KL 501
Dayton, OH 45469-0170

8. PERFORMING ORGANIZATION REPORT NUMBER
UDR-TR-2004-00155

9. SPONSORING/MONITORING AGENCY NAME(S) AND ADDRESS(ES)

Propulsion Directorate
Air Force Research Laboratory
Air Force Materiel Command
Wright-Patterson AFB, OH 45433-7251

10. SPONSORING/MONITORING AGENCY ACRONYM(S)
AFRL/PRPS

11. SPONSORING/MONITORING AGENCY REPORT NUMBER(S)
AFRL-PR-WP-TP-2005-200

12. DISTRIBUTION/AVAILABILITY STATEMENT
Approved for public release; distribution is unlimited.

13. SUPPLEMENTARY NOTES

Report contains color. This report is comprised of two journal articles and one conference paper.

14. ABSTRACT
The purpose of this effort was the basic advancement of high temperature solid oxide fuel cell electrolyte technology.

15. SUBJECT TERMS
fuel cell, solid oxide, electrolyte, yttria, electrical, conductivity, scandia

16. SECURITY CLASSIFICATION OF:			17. LIMITATION OF ABSTRACT:	18. NUMBER OF PAGES	19a. NAME OF RESPONSIBLE PERSON (Monitor)
a. REPORT	b. ABSTRACT	c. THIS PAGE			Joseph P. Fellner
Unclassified	Unclassified	Unclassified	SAR	52	19b. TELEPHONE NUMBER *(Include Area Code)* (937) 255-4225

Standard Form 298 (Rev. 8-98)
Prescribed by ANSI Std. Z39-18

TABLE OF CONTENTS

FUEL CELLS FOR AEROSPACE POWER

1. INTRODUCTION

During the course of this program, electrical properties of heterogeneously doped yttria stabilized zirconia (YSZ) and Scandia stabilized zirconia (ScSZ) have been characterized. In both cases, the heterogeneous dopant was alumina (Al_2O_3). These materials were prepared using conventional ceramic processing techniques such as mixing, pressing and sintering. A detailed analysis of the specimen properties have been published in three publications which are listed below and also provided as appendices.

1. "Electrical properties of heterogeneously doped yttria stabilized zirconia," B. Kumar, C. Chen, C. Varanasi, and J.P. Fellner, *J. Power Sources* (2004). [Appendix A]
2. "Electrical Properties of Yttria Stabilized Zirconia and Alumina Composites," B. Kumar, C. Chen, C. Varanasi, and J.P. Fellner, Proceedings of the Electrochemical Society Symposium of Ionic and Mixed Ion Conductors, Honolulu, Hawaii, October 3-8, 2004. [Appendix B]
3. "Electrical Conductivity Enhancement in Heterogeneously Doped Scandia Stabilized Zirconia," to be published in the *J. of Electrochem. Soc.* (2005). [Appendix C]

Appendix A

DTD 5

ARTICLE IN PRESS

Available online at www.sciencedirect.com

SCIENCE DIRECT®

ELSEVIER

Journal of Power Sources xxx (2004) xxx–xxx

JOURNAL OF POWER SOURCES

www.elsevier.com/locate/jpowsour

Electrical properties of heterogeneously doped yttria stabilized zirconia

Binod Kumar[a,*], Christina Chen[a], Chakrapani Varanasi[a], Joseph P. Fellner[b]

[a] *Metals and Ceramics Division, University of Dayton Research Institute, 300 College Park, Dayton, OH 45469-0170, USA*
[b] *Propulsion Directorate, Air Force Research Laboratory, Wright-Patterson AFB, OH 45433-7251, USA*

Received 26 July 2004; accepted 15 August 2004

Abstract

This paper reports the effects of heterogeneously doped Al_2O_3 on the ionic conductivity of yttria stabilized zirconia (YSZ). At lower dopant concentration, grain growth occurred and the grain boundaries were re-formed. Subsequent increases in the dopant concentration decreased the grain size. The doping leads to the creation of space charge regions in the vicinity of the YSZ–Al_2O_3 boundaries, conducive to enhanced transport of oxygen ions. The presence of Al_2O_3 also leads to a blocking effect. The net result of the two antagonistic influences is small and reflected by a relatively minor influence on conductivity.

Keywords: Dopant; Zirconia; Ionic conductivity

1. Introduction

Ionic conductivity and microstructure are critical parameters of an electrolyte for its application in a solid oxide fuel cell (SOFC). The ionic conductivity determines, to a large extent, the available power and operating temperature of a SOFC, whereas the microstructure is of vital importance and critical for mechanical properties, including long-term survivability of the electrolyte. The ionic conductivity of a stabilized zirconium oxide depends upon the concentration and mobility of oxygen vacancies, which in turn are closely linked to the dopant concentration. A dopant (Ca^{2+}, Y^{3+}, etc.) concentration higher than the optimum may reduce the number of mobile oxygen ions because of defect association and the resulting ionic conductivity. These homogeneously doped, stabilized zirconia are the mainstay electrolytes in state-of-the-art SOFCs.

The electrical conductivity of stabilized zirconia is explained by the so-called 'brick layer model.' [1] The model postulates the existence of cubic grains of stabilized zirconia uniformly dispersed within homogeneous grain boundaries. The grain boundaries are more resistive than the grains—the grain boundary conductivity (inverse of resistivity) is about two orders of magnitude lower than the grain conductivity. Thus, the bulk conductivity of stabilized zirconia is primarily determined by the weak link, grain boundary conductivity. To improve power density or reduce the operating temperature of a SOFC, the conductivity of the bulk electrolytes needs to be enhanced. To achieve this objective, the grain boundary conductivity must be increased.

A number of different approaches can be employed to enhance conductivity of the bulk electrolyte. For example, a rare earth dopant with an ionic radius closer to the host zirconium, such as scandium, is known to enhance grain conductivity, but the grain boundary conductivity remains unaffected. An alternate route to enhance bulk conductivity of stabilized zirconia is to employ a heterogeneous dopant. These heterogeneous dopants are insoluble in host yttria stabilized zirconia (YSZ) and remain the physically distinct phase of the bulk structure. For a number of ionic conductors, it has been demonstrated that the existence of an inert, heterogeneous dielectric phase in a conducting matrix can raise the ionic conductivity by orders of magnitude [2–8].

* Corresponding author. Tel.: +1 937 229 3452; fax: +1 937 229 3433.
E-mail address: kumar@udri.udayton.edu (B. Kumar).

0378-7753/$ – see front matter © 2004 Published by Elsevier B.V.
doi:10.1016/j.jpowsour.2004.08.016

In a pioneering work, Liang [2] investigated polycrystalline lithium iodide doped with aluminum oxide and reported that lithium iodide doped with 35–45 mol% aluminum oxide exhibited conductivity on the order of 10^{-5} S cm^{-1} at 25 °C, about three orders of magnitude higher than that of the LiI conductivity. However, no significant amount of aluminum oxide was determined to be soluble in LiI; thus, the conductivity enhancement could not be explained by the classical doping mechanism and creation of Schottky defects such as in the LiI–CaF_2 system. Subsequently, a number of investigations have reported enhanced conductivity of silver in the AgI–I_2O_3 system, [3] copper in the CuCl–Al_2O_3 system, [4] fluorine in the PbF_2–SiO_2 and PbF_2–Al_2O_3 systems, [5] and lithium in polymer–ceramic composite electrolytes [6]. Four review papers [7–10] also document the developmental history and general characteristics of these fast ionic conductors. Analyses of these reviews point out that a new conduction mechanism evolves which augments the bulk conductivity of single-phase ionic conductors. The new conduction mechanism uses interfacial and/or space charge regions between the two primary components. The interfacial or space charge regions are formed because of the creation of charged vacancies and adsorption/desorption of ions. In effect, these regions are electrically active, which influences transport of conducting ions.

The electrical, mechanical, and thermal properties of stabilized zirconia and alumina composites have been studied by a number of investigators [11–16]. Radford and Bratton [11] investigated electrical conductivity of calcia stabilized zirconia (CSZ) containing 2 mol% Al_2O_3. It was found to be insoluble in the CSZ and segregated at the grain boundaries. The addition of Al_2O_3 lowered the electrical conductivity. Verkerk et al. [12] reported the effects of low concentrations of Fe_2O_3, Al_2O_3, and Bi_2O_3 doping on the sintering behavior of YSZ. These dopants were found to have a negative influence on both the grain and grain boundary conductivities. Butler and Drennan [13] analyzed the microstructure of stabilized zirconia as influenced by Al_2O_3 additions. They suggested that Al_2O_3 acted as a scavenger for SiO_2, removing the silicious phase from grain boundary localities. Miyayama et al. [14] reported that up to 0.5 mol% of Al_2O_3 was found to be soluble in stabilized zirconias. They suggested that Al_2O_3 additions have dual roles: below the solubility limit, grain and grain boundary resistivities increase and grain growth is promoted, whereas the reverse is true above the solubility limit of Al_2O_3; i.e., grain boundary resistivity decreases and grain growth is inhibited. However, Miyayama et al. [14] investigated Al_2O_3 additions only up to 1 mol%. Mori et al. [15] characterized mechanical, thermal, and electrical properties of 8 mol% stabilized zirconia with Al_2O_3 doping. The strength of the composites increased with increasing Al_2O_3 content up to 20 wt.%. The thermal conductivity of the composite increased, whereas the coefficient of thermal expansion decreased with increasing Al_2O_3 content. They observed a slight increase in electrical conductivity up to 1 wt.% and subsequently a monotonic decrease with increasing Al_2O_3 content. The electrical conductivity of 8YSZ doped with 20 wt.% Al_2O_3 was reported to be 0.1 S cm^{-1} at 1000 °C. The effect of Al_2O_3 additions upon the electrical conductivity of 8 mol% YSZ was also investigated by Feighery and Irvine [16]. They reported that approximately 1 wt.% Al_2O_3 dissolves into the structure of YSZ when sintered at 1500 °C for 24 h. Furthermore, the high-temperature conductivity increases for 1 wt.% Al_2O_3 and then decreases to approximately the same conductivity as the undoped 8YSZ. The conductivity remained constant until 10 wt.% Al_2O_3 and subsequently decreased rapidly with further addition of Al_2O_3.

Guo et al. [1,17,18] reported an analysis of the contributions of grain and grain boundaries to the total electrical conductivities of stabilized zirconias. The grain boundaries constituting the core (crystallographic mismatch zone) and space charge regions in stabilized zirconias impede ionic transport across them. The grain boundary resistivity is normally several orders of magnitude greater than the grain resistivity. The resistive grain boundaries have been linked to the impurities, particularly the silicious phase, for a long time. But even in highly pure stabilized zirconias, the grain boundary resistivity was still found to be several orders of magnitude greater than the grain resistivity. Therefore, Guo et al. [18] questioned the proposed origin of the grain boundary resistivity and suggested that the resistive grain boundaries can be explained on the basis of space charges and depletion of oxygen vacancies in the vicinity of grain boundaries. Guo et al. [18] further reported that the addition of Al_2O_3 in small amounts (0.4 mol%) increased both grain and grain boundary resistivities. The grain resistivity was increased by only 3%, whereas the grain boundary resistivity was increased by 600%.

This paper is a culmination of the vast experimental evidence gathered on the role of the heterogeneous doping on the ionic conductivity of composite solids. The effect of nanosized Al_2O_3 doping on the microstructure and conductivity of yttria stabilized zirconia will be investigated, analyzed, and discussed. The Al_2O_3 dopant was selected because of its use in prior literature (although conflicting observations were reported). It is also known to be insoluble in stabilized zirconia in higher concentrations. A large difference in the ionic radii of aluminum and zirconium leads to a very limited solid solubility between the host ZrO_2 and Al_2O_3. Thus, Al_2O_3 is expected to remain a physically distinct phase (heterogeneous) in the bulk structure of stabilized zirconia. By doping with nanosize Al_2O_3, it is expected that the grain boundary resistivity will be affected.

2. Experimental procedure

A quantity of 8 mol% yttria stabilized zirconia obtained from Tosoh Corporation[1] was mixed with nanosize (24 nm)

[1] 4560 Kaisei-Cho, Shinnanyo-shi, Yamaguchi-Ken 746-8501, Japan.

Table 1
Compositions and densities of heterogeneously doped YSZ

Al_2O_3 (wt.%)	Al_2O_3 (mol%)	Density (g cm^{-3})		Theoretical density (g cm^{-3})
		1500 °C	1520 °C	
0	0	5.83	5.96	5.96
2	2.56	5.59	5.92	5.92
4	5.10	5.41	5.77	5.88
6	7.60	5.25	5.67	5.84
10	12.53	5.04	5.50	5.76
15	18.53	4.86	5.18	5.66
20	24.37	4.75	5.02	5.56

alumina obtained from NanoTek.[2] The batch compositions, as shown in Table 1, were mixed in a mortar and pestle and subsequently pressed into discs (1.27 cm in diameter and 0.15 cm thick) with a pressure of 2.5 ton cm^{-2} and then sintered at 1500–1520 °C for 4 h. The densities of sintered specimens were measured by the Archimedes principle. The electrical conductivity of each specimen was measured by the ac and dc techniques in the 300–975 °C temperature range. For the ac technique, a Solartron 1260 impedance analyzer with 1287 electrochemical interface was used to obtain impedance data in the 0.1–10^6 Hz frequency range. The specimen with the highest density for a given composition (corresponding to a sintering temperature of 1520 °C) was characterized by the ac technique. The two surfaces of each specimen were covered with platinum foils and placed in the cell fixture under a pressure applied by tightening the screw of the cell fixture.[3] The assembled cell fixture was placed in a furnace and an impedance measurement was conducted as a function of temperature. The dc resistances of these specimens were also measured as a function of temperature using a Fluke multimeter.

The microstructure was investigated by means of scanning electron microscopy (SEM, JEOL Model JSM-840). The SEM studies were conducted on polished and thermally etched surfaces, and the average grain size was determined by counting the grains and dividing by the area.

A Rigaku Ratablex RV-200BH X-ray diffractometer was used to obtain power diffraction patterns of the specimens. The sintered specimens were ground into powder and subsequent X-ray diffraction (XRD) patterns were obtained. The diffractometer was operated at 40 kV, 15 mA with copper target.

[2] Nanophase Technologies Corporation, 8205 S. Cass Ave. #105, Darien, IL 60561.

[3] Since all specimens were characterized by the same method, the trend in conductivity variation with composition can be compared and analyzed. The absolute values of the conductivities are expected to be different as compared to the literature, since different experimental conditions were used in the present investigation.

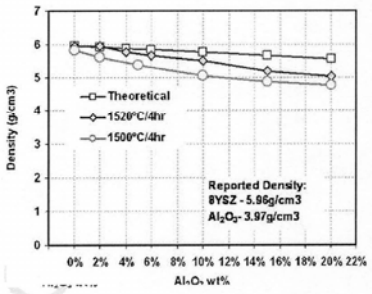

Fig. 1. Density of YSZ vs. wt.% of Al_2O_3.

3. Results and discussion

3.1. Density

Fig. 1 presents plots of theoretical and sintered densities of specimens as a function of Al_2O_3 concentration. Since the density of Al_2O_3, 3.97 g cm^{-3}, is lower than the density of the stabilized zirconia, densities of all doped specimens decrease with the concentration of the dopant. An increase in the sintering temperature by 20 °C leads to a significant enhancement in density at all concentrations, with the measured density over 90% of the theoretical density. It is interesting to note that at a 20% dopant level, the electrolyte density is reduced over 16%, which is expected to have a positive influence on the power densities of fuel cell stacks containing these doped electrolytes.

3.2. Microstructure

The microstructures of five specimens containing 0, 4, 6, 10, and 20 wt.% Al_2O_3 are shown in Fig. 2(a–e), respectively. The microstructure of the undoped YSZ (Fig. 2(a)) is typical of the material and shows the presence of pores within the grains. These pores appear as dark, concave spherical regions in the micrograph. The grain boundaries are distinct and do not exhibit the presence of an excessive, seg-

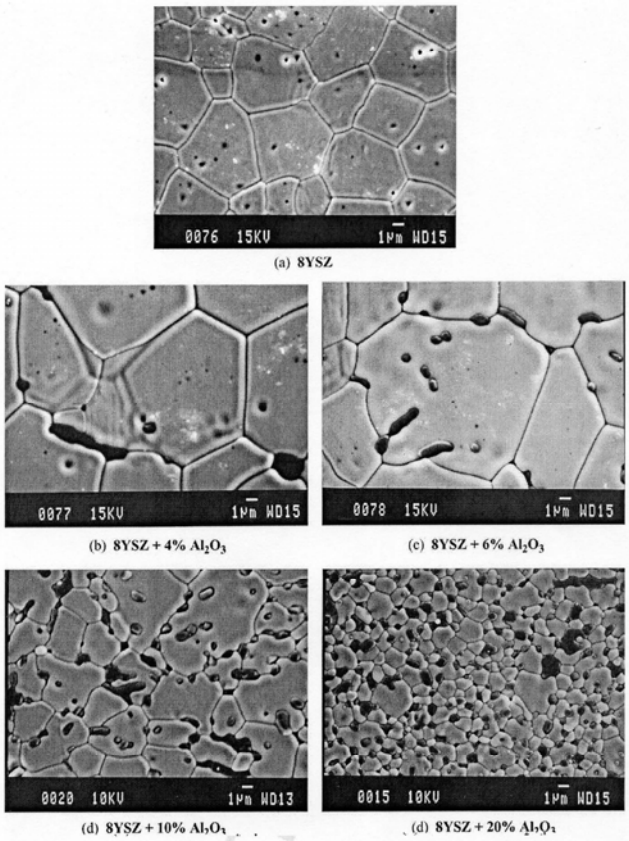

(a) 8YSZ

(b) 8YSZ + 4% Al_2O_3

(c) 8YSZ + 6% Al_2O_3

(d) 8YSZ + 10% Al_2O_3

(d) 8YSZ + 20% Al_2O_3

Fig. 2. SEM microstructure of 8YSZ with Al_2O_3 addition from 0 to 20 wt.%.

regated impurity phase. With the addition of 4 wt.% Al_2O_3, grain growth occurred and the Al_2O_3 phase as shown by the dark areas segregated at the grain boundaries (Fig. 2(b)). The Al_2O_3 precipitates can also be observed inside the grains. The structure of the grain boundaries in Fig. 2(b) suggests that they have been re-formed. The microstructure exhibits well-defined triple points with almost linear grain boundaries. The Al_2O_3 acts as a sintering aid, and the sintering appears to occur by dissolution and precipitation. The solubilities of Al_2O_3 in the grain and grain boundaries re-form the microstructure of the YSZ. The excess Al_2O_3 is precipitated primarily at the grain boundaries. Increasing the Al_2O_3 concentration to 6% leads to further grain growth (Fig. 2(c)) and the presence of the Al_2O_3 phase along the grain boundaries and grain cavity. The presence of Al_2O_3 in cavities is characterized by convex surfaces. At this concentration of Al_2O_3, a linear as well as isolated droplet-like morphology of the dopant are noted. As the concentration of Al_2O_3 increased to 10 wt.%, there is a substantial increase in the volume fraction of this phase (Fig. 2(d)) which exists at grain boundaries and also as distinct grains. The average grain size of the YSZ has been reduced. The 20 wt.% Al_2O_3 specimen (Fig. 2(e)) shows further reduction in the average grain size and the microstructure is on the threshold of transitioning into a nanostructure.

Analyses of all the micrographs shown in Fig. 2(a–e) reveal that the two phases; i.e., YSZ and Al_2O_3, are immiscible

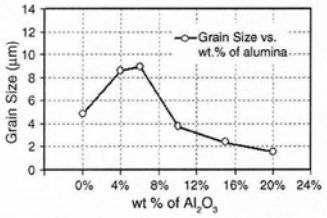

Fig. 3. Grain size vs. Al_2O_3 content (sintered at 1520 °C for 4 h).

at significant concentrations and possess very different surface energies. The Al_2O_3 exhibits non-wettable characteristics on the YSZ substrate.

The average grain size as a function of Al_2O_3 concentration is presented in Fig. 3. As stated earlier, the YSZ grain growth occurs up to about 6 wt.%. This observation is contrary to the reports of Miyayama et al. [14] who observed grain growth until only up to about 0.5 wt.% of Al_2O_3. The dissolution of Al_2O_3 in YSZ in small amounts led to the grain growth. The nanosize Al_2O_3 was introduced to the YSZ. Nonetheless, the size of Al_2O_3 along the grain boundary in the order of several microns in micrographs (Fig. 2(b–c)) may have formed by dissolution, precipitation, and coarsening. Further addition of Al_2O_3 up to 20 wt.% retards grain growth (Fig. 2(d–e)). The 20 wt.% Al_2O_3 material exhibits a morphology with an average grain size of 1.4 μm.

3.3. X-ray diffraction

XRD patterns from undoped and doped (4, 10, and 20%) YSZ are shown in Fig. 4. There is no apparent shift in the d-spacings noted due to the addition of Al_2O_3, which suggests that there is a very limited solid solubility between the two phases. New diffraction peaks corresponding to Al_2O_3 begin to appear in the 4 wt.% specimens and become much stronger for 10–20 wt.% specimens. The d-spacings of these specimens are also presented in Table 2, which clearly shows that the specimens are basically mechanical mixtures of the two components and comply with the definition of heterogeneous doping.

Table 2
d-Spacings of undoped and doped YSZ

Undoped	Doped		
	4% Al_2O_3	10% Al_2O_3	20% Al_2O_3
2.9614 (YSZ)	2.9616 (YSZ)	2.9698 (YSZ)	2.9611 (YSZ)
2.5649 (YSZ)	2.5669 (YSZ)	2.5712 (YSZ)	2.5648 (YSZ)
	2.3757 (Al_2O_3)	2.3799 (Al_2O_3)	2.3751 (Al_2O_3)
	2.0823 (Al_2O_3)	2.0853 (Al_2O_3)	2.0812 (Al_2O_3)
1.8152 (YSZ)	1.8153 (YSZ)	1.8173 (YSZ)	1.8143 (YSZ)
		1.7399 (Al_2O_3)	1.7369 (Al_2O_3)
		1.6013 (Al_2O_3)	1.5999 (Al_2O_3)
1.5484 (YSZ)	1.5485 (YSZ)	1.5498 (YSZ)	1.5477 (YSZ)
1.4825 (YSZ)	1.4826 (YSZ)	1.4837 (YSZ)	1.4817 (YSZ)
		1.4042 (Al_2O_3)	1.4030 (Al_2O_3)
		1.3737 (Al_2O_3)	1.3722 (Al_2O_3)
1.2839 (YSZ)	1.2841 (YSZ)	1.2850 (YSZ)	1.2842 (YSZ)

3.4. Oxygen-ion conductivity

A schematic of an equivalent circuit representing a bulk structure of the specimens and corresponding ac impedance response as presented by a plot of real versus imaginary parts of the impedance is shown in Fig. 5. The equivalent circuit consists of a resistor representing contract resistance, a second resistor connected with a capacitor in parallel depicting the ceramic grain and a third resistor with a capacitor in parallel portraying the grain boundaries. The ac response is characterized by the existence of two adjoining semicircles slightly shifted from origin. The magnitude of the shift on the real axis (Z′) represents resistance of the electrolyte–electrode contacts. The first semicircle next to the contact resistance depicts the electrical properties (resistance and capacitance)

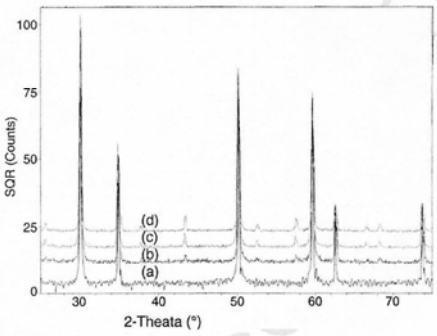

Fig. 4. X-ray diffraction patterns from Al_2O_3 doped YSZ: (a) undoped YSZ, (b) 4 wt.% Al_2O_3–YSZ, (c) 10 wt.% Al_2O_3–YSZ, (d) 20 wt.% Al_2O_3–YSZ.

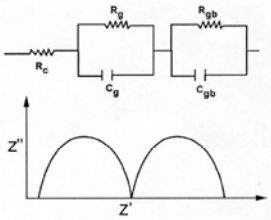

Fig. 5. Schematic equivalent circuit and ac impedance response of a bulk YSZ.

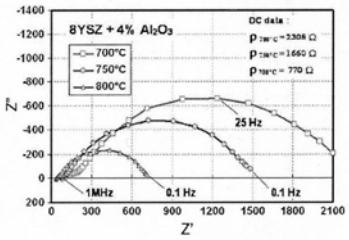

Fig. 6. AC impedance measurement plots at 700–800 °C for 8YSZ + 4% Al_2O_3.

of ceramic grains and the second semicircle represents characteristics of the grain boundary. A simulation study comprised of breadboard circuits and software analysis suggests that the ratio of grain capacitance (C_g) to grain boundary capacitance (C_{gb}) must be less than 10^{-3} for the existence of two semicircles, whereas the ratio of grain resistance (R_g) to grain boundary resistance (R_{gb}) does not matter. If the ratio of C_g:C_{gb} is greater than 10^{-3}, the presence of only one semicircle is predicted.

Typical experimental impedance measurement data for the 4 wt.% Al_2O_3 doped specimen at 700, 750, and 800 °C in the frequency range of 0.1–10^6 Hz are shown in Fig. 6. The impedance plot is depicted by a distorted semicircle originating from a non-zero origin on the Z'-axis. The temperature increase shrinks the diameter of the distorted circle, illustrating that the specimen becomes less resistive. The resistance value as determined from the diameter of the distorted semicircle on the Z'-axis is also approximately equal to the dc resistance measured by a multimeter (also shown in Fig. 6). The impedance plot of the 10 wt.% Al_2O_3 specimen at 850 °C (Fig. 7) shows three resistance parameters, R_1, R_2, and R_{Total}. The R_1 parameter corresponds to the contact resistance whereas $R_2 - R_1$ parameter is the grain resistance. The grain boundary resistance is equal to $R_{Total} - R_2$. These resistances ($R_2 - R_1$ and $R_{Total} - R_2$) were normalized with

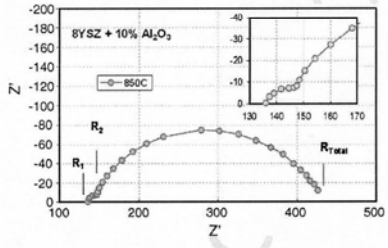

Fig. 7. Determination of resistivities of grain and grain boundary from an ac impedance plot: R_1 is the interface resistance; the grain resistance $R_{grain} = R_2 - R_1$, and the grain boundary resistance $R_{gb} = R_{Total} - R_2$.

specimen geometry (thickness and cross sectional area) to obtain corresponding resistivities (ρ) or conductivities ($\sigma = (1/\rho)$). It should be noted that $R_2 - R_1$ is the diameter of a small semicircle barely discernible (see insert in Fig. 7), implying that the grain possesses both capacitive and resistive elements. The grain boundary of the specimen is characterized by much larger resistive and capacitive elements.

The Arrhenius plots of the grain and grain boundary conductivities of the undoped, 4 and 20 wt.% Al_2O_3 are shown in Fig. 8. It should be noted that the grain conductivity is over an order of magnitude greater than the grain boundary conductivity. The difference between the grain and grain boundary conductivities is less than the value reported for the 8YSZ by Guo et al. [18] The bulk, total conductivity comprised of grain and grain boundary contributions is shown in Fig. 9. Again in this case the data sets are clustered and it appears that the doping concentration up to 20 wt.% Al_2O_3 has decreased the conductivity; however, the dopant appears to have a minor influence.

The observations on the electrical conductivity of the doped specimens of this investigation parallel the observations made by Mori et al. [15] and Feighery and Irvine [16]. Mori et al. [15] reported that the bulk conductivity of 8YSZ doped with Al_2O_3 increased slightly with increasing Al_2O_3 up to 1 wt.%. Furthermore, they reported that the conductivity of 20 wt.% Al_2O_3 was around 0.1 S cm^{-1} at 1000 °C, about 65% of that of the undoped 8YSZ. Mori et al. [15] had doped the 8YSZ with up to 30 wt.% of Al_2O_3 without observing a major drop in ionic conductivity. Similarly, Feigh-

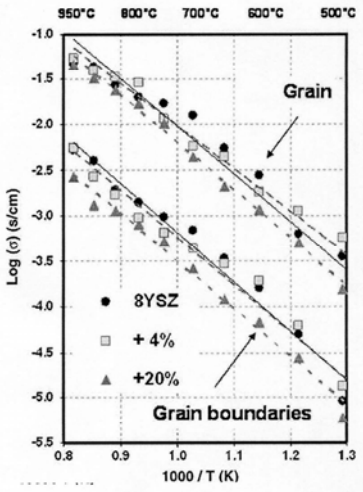

Fig. 8. Conductivity shown as log(σ) vs. 1000 T^{-1} for 8YSZ and 8YSZ + 4–20% alumina.

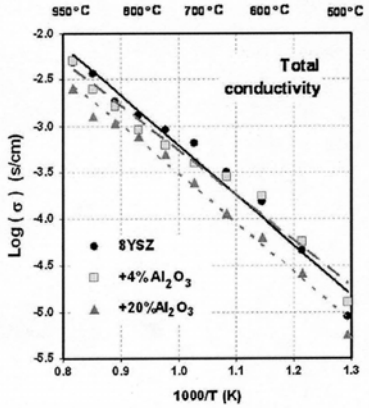

Fig. 9. Arrhenius plots: total conductivity shown as log(σ) vs. 1000 T^{-1} for 8YSZ and 8YSZ + 4–20% alumina.

ery and Irvine [16] had also doped 8YSZ with Al_2O_3 up to 24 wt.%; however, they reported that 10 wt.% Al_2O_3 can be introduced to the 8YSZ without a significant reduction in the ionic conductivity. Further additions of Al_2O_3 caused a rapid reduction in the conductivity, which was rationalized on the basis of the presence of a large volume fraction of insulating Al_2O_3 phase. Neither Mori et al. [15] nor Feighery and Irvine [16] analyzed contributions of grain and grain boundaries independently on the total bulk conductivity in these heavily-doped YSZ–Al_2O_3 composites.

Since there is a major reduction in the ionically conducting (active) phase in these 8YSZ–I_2O_3 composites, a normalized plot of ionic conductivity versus Al_2O_3 may be useful to delineate the effect of Al_2O_3 additions. Normalized conductivity (conductivity of a composite/volume fraction of active phase) in S cm^{-1} of grain, grain boundary, and total conductivities is shown in Fig. 10. The normalized grain conductivity shows an enhancement reaching a peak around 15 wt.% of Al_2O_3. The conductivity enhancement is approximately 30%. The normalized grain boundary conductivity appears to increase initially up to about 4 wt.% and then it gradually decreases. The grain boundary conductivity is lower than the grain conductivity by a factor of 10–15. The bulk total conductivity shows a trend similar to the grain boundary, as it is the dominating factor.

It is of significant relevance to review the effect of inert dopant on the conductivity of an ionically conducting matrix. A general trend on the effect of dopant particles on the ionic conductivity of composites is shown in Fig. 11. With the addition of dopant particles, the ionic conductivity of composites increases and reaches a peak around 20 vol.% of the insulating dopant. Further increases of the dopant decreases the conductivity as it impedes the transport of charged species. A steady-state percolation of the conducting ion occurs around 20 vol.% of the insulating dopant phase leading to an optimum conductivity. The percolation threshold may vary depending upon the matrix dopant chemistries, particle sizes, and processing parameters. The particle size of the dopant has a major influence on the conductivity, which has been reported in earlier publications [6–8].

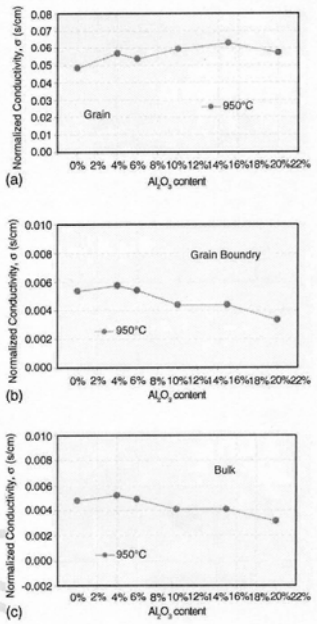

Fig. 10. Normalized conductivity vs. Al_2O_3 content.

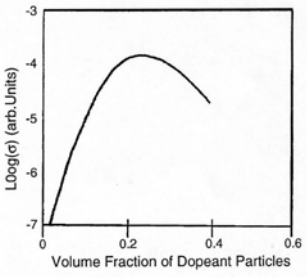

Fig. 11. Low-temperature ionic conductivity of ionically conducting matrix reinforced with insulating particles.

The conductivity data of this investigation does not show a trend characteristic of composite ionic conductors as depicted by Fig. 11 because of: (1) widely different contributions of the grain and grain boundaries to the bulk conductivity of the host material; (2) dissolution, precipitation and grain growth of the dopant phase; and (3) antagonistic influences of the dopant on conductivity. The contributions of grain and grain boundary to total bulk conductivity have been discussed earlier. The dissolution and precipitation of the dopant phase is evident from the microstructures as presented in Fig. 2. Guo and Maier [17] investigated YSZ doped with 0.4 mol% Al_2O_3 in the temperature range of 200–500 °C. Since no Al_2O_3 particles were observed in their SEM images, it was suggested that 0.4 mol% was within the solubility limit. The contribution of Al_2O_3 doping to the grain conductivity was insignificant; however, it drastically decreased the grain boundary conductivity almost by a factor of six. In this investigation, the concentration of Al_2O_3 is much greater and the presence of Al_2O_3 particles primarily at the grain boundaries leads to the formation of space charge regions, which are known to assist transport of charged specie, as in other composite ionic conductors. At the same time, Al_2O_3 particles at larger volume fractions may also impede the transport of the charged specie. Both of these influences on conductivity appear to counteract each other in the specimens investigated in this study. It is known from the work of Guo and Maier [17] that a small amount of Al_2O_3 is detrimental to conductivity. The addition of an excess of Al_2O_3, which is physically present in the structure, should also hinder transport of the conducting ions. These two factors, therefore, should lead to a rapid drop in the conductivity with Al_2O_3 additions. However, experimental evidence from this investigation and also those of Mori et al. [15] and Feighery [16] are contradictory; thus, one is led to conclude that space charge regions at the YSZ–Al_2O_3 phase boundaries are created which augment the transport of oxygen ions, but a distinct conductivity peak is not observed. Thus, it is suggested that the dopant, Al_2O_3, imparts antagonistic influences to the total conductivity.

The resistive grain boundary of YSZ results from the depletion of oxygen vacancies, $V_o^{\bullet\bullet}$, in the vicinity of the grain boundaries. A schematic of concentrations of oxygen vacancies, electrons in YSZ, and electrons in Al_2O_3 doped specimens are schematically shown in Fig. 12(a–c). The creation of oxygen vacancies can be expressed by the Kröger–Vink notation:

$$O_o^x \Leftrightarrow V_o^{\bullet\bullet} + 2e' + \tfrac{1}{2}O_2 \quad (1)$$

The depletion of oxygen vacancies near the grain boundary also leads to an enrichment of electron concentration, which provides an energy barrier to the transport of oxygen ions. It is proposed that Al_2O_3 doping reverses Eq. (1) and the electron concentration gradient is removed (Fig. 12(c)). The experimental data in Fig. 10 that the normalized grain boundary conductivity exhibits a slight enhancement in the early stages of doping and subsequently a gradual reduction attest to the conclusion that the grain boundary conductivity must increase to counteract negative influences of the Al_2O_3 addition.

4. Summary and conclusions

This paper investigated the effects of nanosize Al_2O_3 doping on conductivity of 8 mol% yttria stabilized zirconia. The Al_2O_3 doping concentration was varied from 0 to 20 wt.%

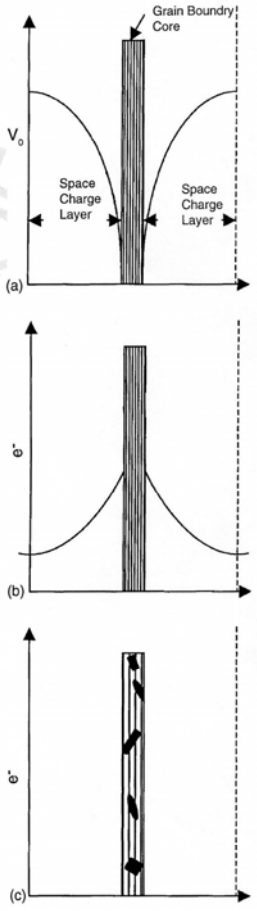

Fig. 12. Schematic profiles of (a) oxygen vacancy, (b) electrons, and (c) electrons in doped YSZ.

and the specimens were characterized by SEM, XRD, and impedance spectroscopy. The significant conclusions of the investigation are summarized as follows:

1. The composite specimens of this investigation were truly heterogeneous as evidenced by SEM micrographs and XRD data. The solid solubility between the YSZ and Al_2O_3 was minimal, as no significant change in the d-spacings occurred.
2. Initially there was a grain growth with the addition of Al_2O_3 up to about 6 wt.%. The grain size increased from 4 to 6 μm and the grain boundaries became sharper. With further addition of Al_2O_3, the grain size decreased to 1.6 μm for 20 wt. Al_2O_3.
3. The conductivity data of the bulk specimen obtained from the ac measurement revealed a minor influence on the total, bulk conductivity due to the addition of Al_2O_3. The conductivity remained relatively flat as the Al_2O_3 content was increased. Both grain and grain boundary conductivities were characterized and their contributions were discussed.
4. The conductivity variation was explained on the basis of antagonistic influences of Al_2O_3 doping. The doping leads to the creation of space charge regions in the vicinity of YSZ–Al_2O_3 boundaries, which should enhance transport of oxygen ions and thus conductivity. The presence of Al_2O_3 may also lead to a blocking effect suppressing conductivity. The net effect of the two antagonist influences is small and reflected by a relatively flat conductivity as the concentration of Al_2O_3 was increased.

Acknowledgment

Three of the authors gratefully acknowledge the financial support by the Air Force Research Laboratory, Propulsion Directorate, under Contract No. F33615-02-D-2299.

References

[1] X. Guo, Y. Ding, J. Electrochem. Soc. 151 (1) (2004) J1–J7.
[2] C.C. Liang, J. Electrochem. Soc. 120 (1973) 1289.
[3] K. Shahi, J.B. Wagner, Solid State Ionics 3/4 (1981) 295.
[4] T. Jow, J.B. Wagner, J. Electrochem. Soc. 126 (1979) 1963.
[5] K. Hariharan, J. Maier, J. Electrochem. Soc. 142 (10) (1995) 3469.
[6] B. Kumar, S.J. Rodrigues, L.G. Scanlon, J. Electrochem. Soc. 148 (10) (2001) 1191.
[7] R.C. Agrawal, R.K. Gupta, J. Mater. Sci. 34 (1999) 1131.
[8] A. Mikrajuddin, G. Shi, K. Okuyama, J. Electrochem. Soc. 147 (8) (2000) 3157–3165.
[9] P. Knauth, J. Electroceramics 5 (2) (2000) 111–125.
[10] B. Kumar, L.G. Scanlon, J. Power Sources 52 (1994) 261.
[11] K.C. Radford, R.J. Bratton, J. Mater. Sci. 14 (1979) 66–69.
[12] M.J. Verkerk, A.J.A. Winnubst, A.J. Burggraaf, J. Mater. Sci. (17) (1982) 3113–3122.
[13] E.P. Butler, J. Drennan, J. Amer. Ceram. Soc. 65 (10) (1982) 474–478.
[14] M. Miyayama, H. Yanagida, A. Asada, Am. Ceram. Soc. Bull. 64 (1) (1985) 660–664.
[15] M. Mori, T. Abe, H. Itoh, O. Yamamoto, Y. Takeda, T. Kawahara, Solid State Ionics 74 (1994) 157–164.
[16] A.J. Feighery, J.T.S. Irvine, Solid State Ionics 121 (1999) 209–216.
[17] X. Guo, J. Maier, J. Electrochem. Soc. 148 (3) (2001) E121–E126.
[18] X. Guo, W. Sigle, J. Fleig, J. Maier, Solid State Ionics 154–155 (2002) 555–561.

Appendix B

ELECTRICAL PROPERTIES OF YTTRIA STABILIZED ZIRCONIA AND ALUMINA COMPOSITES

Binod Kumar, Christina Chen, and Chakrapani Varanasi
University of Dayton Research Institute, Metals and Ceramics Division
Dayton, OH 45469-0170
and
Joseph P. Fellner
Propulsion Directorate, Air Force Research Laboratory
Wright-Patterson AFB, OH 45433-7251

ABSTRACT

This paper reports the effects of heterogeneously doped Al_2O_3 on the ionic conductivity of yttria stabilized zirconia (YSZ). At lower dopant concentration, grain growth occurred and the grain boundaries were reformed. Subsequent increases in the dopant concentration decreased the grain size. The doping leads to the creation of space charge regions in the vicinity of the YSZ-Al_2O_3 boundaries, conducive to enhanced transport of oxygen ions. The presence of Al_2O_3 also leads to a blocking effect. The net result of the two antagonistic influences is small and reflected by a relatively minor influence on conductivity.

INTRODUCTION

Ionic conductivity and microstructure are critical parameters of an electrolyte for its application in a solid oxide fuel cell (SOFC). The ionic conductivity determines, to a large extent, the available power and operating temperature of a SOFC, whereas the microstructure is of vital importance and critical for mechanical properties, including long-term survivability of the electrolyte. The ionic conductivity of a stabilized zirconium oxide depends upon the concentration and mobility of oxygen vacancies, which in turn are closely linked to the dopant concentration. A dopant (Ca^{2+}, Y^{3+}, etc.) concentration higher than the optimum may reduce the number of mobile oxygen ions because of defect association and the resulting ionic conductivity. These homogeneously doped, stabilized zirconia are the mainstay electrolytes in state-of-the-art SOFCs.

The electrical conductivity of stabilized zirconia is explained by the so-called "brick layer model."[1] The model postulates the existence of cubic grains of stabilized zirconia uniformly dispersed within homogeneous grain boundaries. The grain boundaries are more resistive than the grains – the grain boundary conductivity (inverse of resistivity) is about two orders of magnitude lower than the grain conductivity. Thus, the bulk conductivity of stabilized zirconia is primarily determined by the weak link, grain boundary conductivity. To improve power density or reduce the operating temperature of a SOFC, the conductivity of the bulk electrolytes needs to be enhanced. To achieve this objective, the grain boundary conductivity must be increased.

A number of different approaches can be employed to enhance conductivity of the bulk electrolyte. For example, a rare earth dopant with an ionic radius closer to the host zirconium, such as scandium, is known to enhance grain conductivity, but the grain boundary conductivity remains unaffected. An alternate route to enhance bulk conductivity of stabilized zirconia is to employ a heterogeneous dopant. These heterogeneous dopants are insoluble in host yttria stabilized zirconia (YSZ) and remain as a physically distinct phase of the bulk structure. For a number of ionic conductors, it has been demonstrated that the existence of an inert, heterogeneous dielectric phase in a conducting matrix can raise the ionic conductivity by orders of magnitude.[2-8]

In a pioneering work, Liang[2] investigated polycrystalline lithium iodide doped with aluminum oxide and reported that lithium iodide doped with 35 to 45 mol% aluminum oxide exhibited conductivity on the order of 10^{-5} S cm^{-1} at 25°C, about three orders of magnitude higher than that of the LiI conductivity. However, no significant amount of aluminum oxide was determined to be soluble in LiI; thus, the conductivity enhancement could not be explained by the classical doping mechanism and creation of Schottky defects such as in the LiI-CaF_2 system. Subsequently, a number of investigations have reported enhanced conductivity of silver in the AgI-Al_2O_3 system,[3] copper in the CuCl-Al_2O_3 system,[4] fluorine in the PbF_2-SiO_2 and PbF_2-Al_2O_3 systems,[5] and lithium in polymer-ceramic composite electrolytes.[6] Four review papers[7-10] also document the developmental history and general characteristics of these fast ionic conductors. Analyses of these reviews point out that a new conduction mechanism evolves which augments the bulk conductivity of single-phase ionic conductors. The new conduction mechanism uses interfacial and/or space charge regions between the two primary components. The interfacial or space charge regions are formed because of the creation of charged vacancies and adsorption/desorption of ions. In effect, these regions are electrically active, which influences transport of conducting ions.

The electrical, mechanical, and thermal properties of stabilized zirconia and alumina composites have been studied by a number of investigators.[11-16] Radford and Bratton[11] investigated electrical conductivity of calcia stabilized zirconia (CSZ) containing 2 mol% Al_2O_3. It was found to be insoluble in the CSZ and segregated at the grain boundaries. The addition of Al_2O_3 lowered the electrical conductivity. Verkerk, et al.[12] reported the effects of low concentrations of Fe_2O_3, Al_2O_3, and Bi_2O_3 doping on the sintering behavior of YSZ. These dopants were found to have a negative influence on both the grain and grain boundary conductivities. Butler and Drennan[13] analyzed the microstructure of stabilized zirconia as influenced by Al_2O_3 additions. They suggested that Al_2O_3 acted as a scavenger for SiO_2, removing the silicious phase from grain boundary localities. Miyayama, et al.[14] reported that up to 0.5 mol% of Al_2O_3 was found to be soluble in stabilized zirconias. They suggested that Al_2O_3 additions have dual roles: below the solubility limit, grain and grain boundary resistivities increase and grain growth is promoted, whereas the reverse is true above the solubility limit of Al_2O_3; i.e., grain boundary resistivity decreases and grain growth is inhibited. However, Miyayama, et al.[14] investigated Al_2O_3 additions only up to 1 mol%. Mori, et al.[15] characterized mechanical, thermal, and electrical properties of 8 mol% stabilized zirconia with Al_2O_3 doping. The strength of the composites increased with increasing Al_2O_3 content up to 20 wt%. The thermal conductivity of the composite increased, whereas the coefficient of thermal expansion decreased with increasing Al_2O_3 content. They observed a slight increase in electrical conductivity up to 1 wt% and subsequently a monotonic decrease with increasing Al_2O_3 content. The electrical conductivity of 8YSZ doped with 20 wt% Al_2O_3 was reported to be 0.1 S cm^{-1} at 1000°C. The effect of Al_2O_3 additions upon the electrical conductivity of 8 mol% YSZ was also investigated by Feighery and Irvine.[16] They reported that approximately 1 wt% Al_2O_3 dissolves into the structure of YSZ when sintered at 1500°C for 24 hours. Furthermore, the high temperature conductivity increases for 1 wt% Al_2O_3 then decreases to approximately the same conductivity as the undoped 8YSZ. The conductivity remained constant until 10 wt% Al_2O_3 and subsequently decreased rapidly with further addition of Al_2O_3.

Guo, et al.[1,17,18] reported an analysis of the contributions of grain and grain boundaries to the total electrical conductivities of stabilized zirconias. The grain boundaries constituting the core (crystallographic mismatch zone) and space charge regions in stabilized zirconias impede ionic transport across them. The grain boundary resistivity is normally several orders of magnitude greater than the grain resistivity. The resistive grain boundaries have been linked to the impurities, particularly the silicious phase, for a long time. But even in highly pure stabilized zirconias, the grain boundary resistivity was still found to be several orders of magnitude greater than the grain resistivity. Therefore, Guo, et al.[18] questioned the proposed origin of the grain boundary resistivity and suggested that the resistive grain boundaries can be explained on the basis of space charges and depletion of oxygen vacancies in the vicinity of grain boundaries. Guo, et al.[18] further reported that the addition of Al_2O_3 in small amounts (0.4 mol%) increased both grain and grain boundary resistivities. The grain resistivity was increased by only 3%, whereas the grain boundary resistivity was increased by 600%.

This paper is a culmination of the vast experimental evidence gathered on the role of the heterogeneous doping on the ionic conductivity of composite solids. The effect of nanosized Al_2O_3 doping on the microstructure and conductivity of yttria stabilized zirconia will be investigated, analyzed, and discussed.

The Al_2O_3 dopant was selected because of its use in prior literature (although conflicting observations were reported). It is also known to be insoluble in stabilized zirconia in higher concentrations. A large difference in the ionic radii of aluminum and zirconium leads to a very limited solid solubility between the host ZrO_2 and Al_2O_3. Thus, Al_2O_3 is expected to remain a physically distinct phase (heterogeneous) in the bulk structure of stabilized zirconia. By doping with nanosize Al_2O_3, it is expected that the grain boundary resistivity will be affected.

EXPERIMENTAL PROCEDURE

A quantity of 8 mol% yttria stabilized zirconia obtained from Tosoh Corporation[1] was mixed with nanosize (24 nm) alumina obtained from NanoTek[2]. The batch compositions were mixed in a mortar and pestle and subsequently pressed into discs (1.27 cm in diameter and 0.15 cm thick) with a pressure of 2.5 ton/cm^2 and then sintered at 1500 to 1520°C for 4 hours. The densities of sintered specimens were measured by the Archimedes principle. The electrical conductivity of each specimen was measured by the ac and dc techniques in the 300 to 975°C temperature range. For the ac technique, a Solartron 1260 impedance analyzer with 1287 electrochemical interface was used to obtain impedance data in the 0.1 to 10^6 Hz frequency range. The specimen with the highest density for a given composition (corresponding to a sintering temperature of 1520°C) was characterized by the ac technique. The two surfaces of each specimen were covered with platinum foils and placed in the cell fixture under a pressure applied by tightening the screw of the cell fixture.[3] The assembled cell fixture was placed in a furnace and an impedance measurement was conducted as a function of temperature. The dc resistances of these specimens were also measured as a function of temperature using a Fluke multimeter.

The microstructure was investigated by means of scanning electron microscopy (SEM, JEOL Model JSM-840). The SEM studies were conducted on polished and thermally etched surfaces, and the average grain size was determined by counting the grains and dividing by the area.

A Rigaku Ratablex RV-200BH x-ray diffractometer was used to obtain power diffraction patterns of the specimens. The sintered specimens were ground into powder and subsequent x-ray diffraction (XRD) patterns were obtained. The diffractometer was operated at 40 kV, 15 mA with copper target.

RESULTS AND DISCUSSION

Density

Figure 1 presents plots of theoretical and sintered densities of specimens as a function of Al_2O_3 concentration. Since the density of Al_2O_3, 3.97 g/cm^3, is lower than the density of the stabilized zirconia, densities of all doped specimens decrease with the concentration of the dopant. An increase in the sintering temperature by 20°C leads to a significant enhancement in density at all concentrations, with the measured density over 90% of the theoretical density. It is interesting to note that at a 20% dopant level, the electrolyte density is reduced over 16%, which is expected to have a positive influence on the power densities of fuel cell stacks containing these doped electrolytes.

[1] 4560 Kaisei-Cho, Shinnanyo-shi, Yamaguchi-Ken 746-8501, Japan.
[2] Nanophase Technologies Corporation, 8205 S. Cass Ave. #105, Darien, IL 60561.
[3] Since all specimens were characterized by the same method, the trend in conductivity variation with composition can be compared and analyzed. The absolute values of the conductivities are expected to be different as compared to the literature, since different experimental conditions were used in the present investigation.

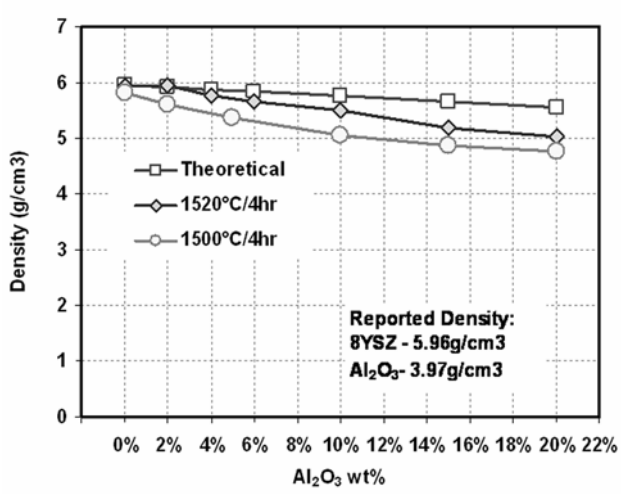

Figure 1. Density of YSZ vs. wt% of Al_2O_3.

Microstructure

The microstructures of five specimens containing 0, 4, 6, 10, and 20 wt% Al_2O_3 are shown in Figures 2 (a) - (e), respectively. The microstructure of the undoped YSZ, Figure 2(a), is typical of the material and shows the presence of pores within the grains. These pores appear as dark, concave spherical regions in the micrograph. The grain boundaries are distinct and do not exhibit the presence of an excessive, segregated impurity phase. With the addition of 4 wt% Al_2O_3, grain growth occurred and the Al_2O_3 phase as shown by the dark areas segregated at the grain boundaries, Figure 2(b). The Al_2O_3 precipitates can also be observed inside the grains. The structure of the grain boundaries in Figure 2(b) suggests that they have been re-formed. The microstructure exhibits well-defined triple points with almost linear grain boundaries. The Al_2O_3 acts as a sintering aid, and the sintering appears to occur by dissolution and precipitation. The solubilities of Al_2O_3 in the grain and grain boundaries re-form the microstructure of the YSZ. The excess Al_2O_3 is precipitated primarily at the grain boundaries. Increasing the Al_2O_3 concentration to 6% leads to further grain growth, Figure 2(c), and the presence of the Al_2O_3 phase along the grain boundaries and grain cavity. The presence of Al_2O_3 in cavities is characterized by convex surfaces. At this concentration of Al_2O_3, a linear as well as isolated droplet-like morphology of the dopant are noted. As the concentration of Al_2O_3 increased to 10 wt%, there is a substantial increase in the volume fraction of this phase, Figure 2(d) which exists at grain boundaries and also as distinct grains. The average grain size of the YSZ has been reduced. The 20 wt% Al_2O_3 specimen, Figure 2(e) shows further reduction in the average grain size and the microstructure is on the threshold of transitioning into a nanostructure.

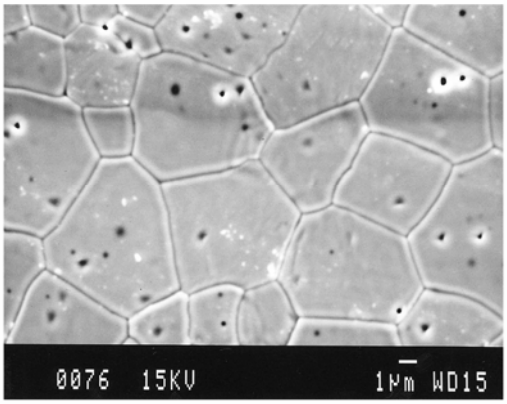

(a) 8YSZ

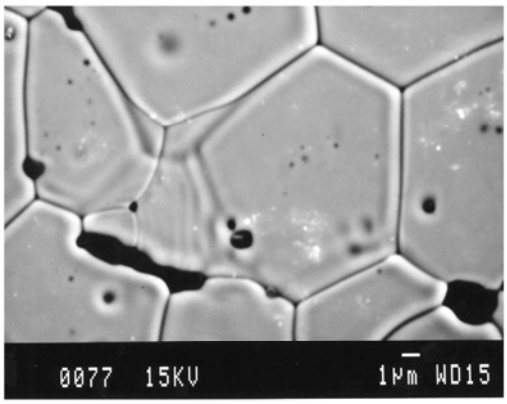

(b) 8YSZ + 4% Al_2O_3

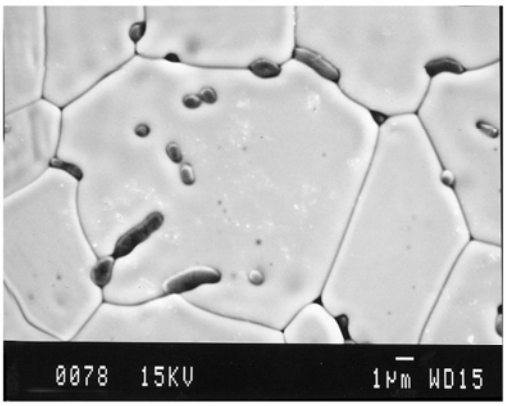

(c) 8YSZ + 6% Al_2O_3

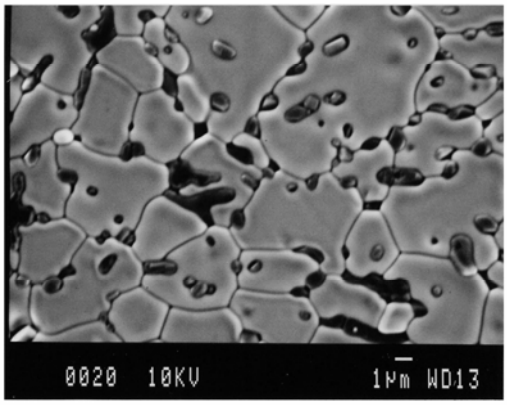

(d) 8YSZ + 10% Al_2O_3

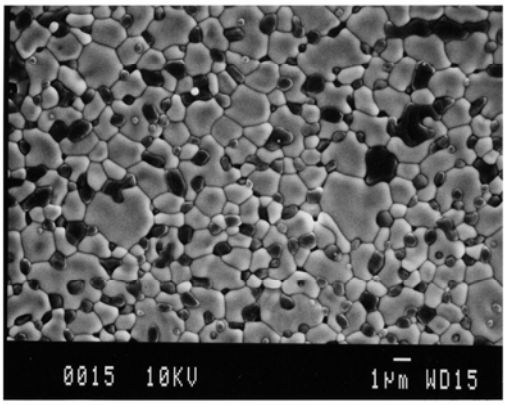

(e) 8YSZ + 20% Al_2O_3

Figure 2. SEM microstructure of 8YSZ with Al_2O_3 addition from 0 to 20 wt%.

Analyses of all the micrographs shown in Figures 2 (a) - (e), reveal that the two phases; i.e., YSZ and Al_2O_3, are immiscible at significant concentrations and possess very different surface energies. The Al_2O_3 exhibits non-wettable characteristics on the YSZ substrate.

The average grain size as a function of Al_2O_3 concentration is presented in Figure 3. As stated earlier, the YSZ grain growth occurs up to about 6 wt%. This observation is contrary to the reports of Miyayama, et al.[14] who observed grain growth until only up to about 0.5 wt% of Al_2O_3. The dissolution of Al_2O_3 in YSZ in small amounts led to the grain growth. The nanosize Al_2O_3 was introduced to the YSZ. Nonetheless, the size of Al_2O_3 along the grain boundary on the order of several microns in micrographs, Figures 2 (b) - (c), may have formed by dissolution, precipitation, and coarsening. Further addition of Al_2O_3 up to 20 wt% retards grain growth, Figure 2(d-e). The 20 wt% Al_2O_3 material exhibits a morphology with an average grain size of 1.4 μm.

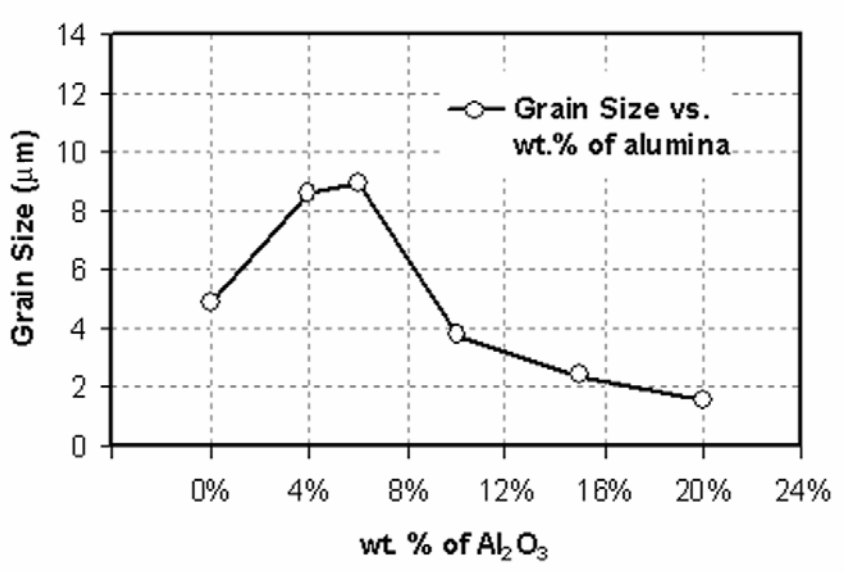

Figure 3. Grain size vs. Al_2O_3 content (sintered at 1520°C for 4 hours).

X-Ray Diffraction

XRD patterns from undoped and doped (4%, 10%, and 20%) YSZ are shown in Figure 4. There is no apparent shift in the d-spacings noted due to the addition of Al_2O_3, which suggests that there is a very limited solid solubility between the two phases. New diffraction peaks corresponding to Al_2O_3 begin to appear in the 4 wt% specimens and become much stronger for 10 to 20 wt% specimens. The XRD data clearly show that the specimens are basically mechanical mixtures of the two components and comply with the definition of heterogeneous doping.

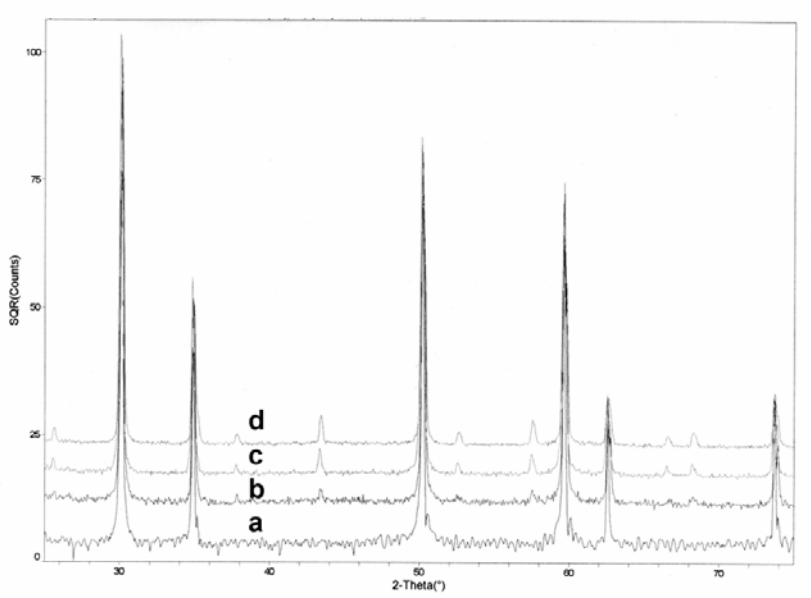

Figure 4. X-ray diffraction patterns from Al_2O_3 doped YSZ: (a) undoped YSZ, (b) 4 wt% Al_2O_3-YSZ, (c) 10 wt% Al_2O_3-YSZ, (d) 20 wt% Al_2O_3-YSZ.

Oxygen-Ion Conductivity

A schematic of an equivalent circuit representing a bulk structure of the specimens and corresponding ac impedance response as presented by a plot of real versus imaginary parts of the impedance is shown in Figure 5. The equivalent circuit consists of a resistor representing contact resistance, a second resistor connected with a capacitor in parallel depicting the ceramic grain and a third resistor with a capacitor in parallel portraying the grain boundaries. The ac response is characterized by the existence of two adjoining semicircles slightly shifted from origin. The magnitude of the shift on the real axis (Z') represents resistance of the electrolyte-electrode contacts. The first semicircle next to the contact resistance depicts the electrical properties (resistance and capacitance) of ceramic grains and the second semicircle represents characteristics of the grain boundary. A simulation study comprised of breadboard circuits and software analysis suggests that the ratio of grain capacitance (C_g) to grain boundary capacitance (C_{gb}) must be less than 10^{-3} for the existence of two semicircles, whereas the ratio of grain resistance (R_g) to grain boundary resistance (R_{gb}) does not matter. If the ratio of C_g:C_{gb} is greater than 10^{-3}, the presence of only one semicircle is predicted.

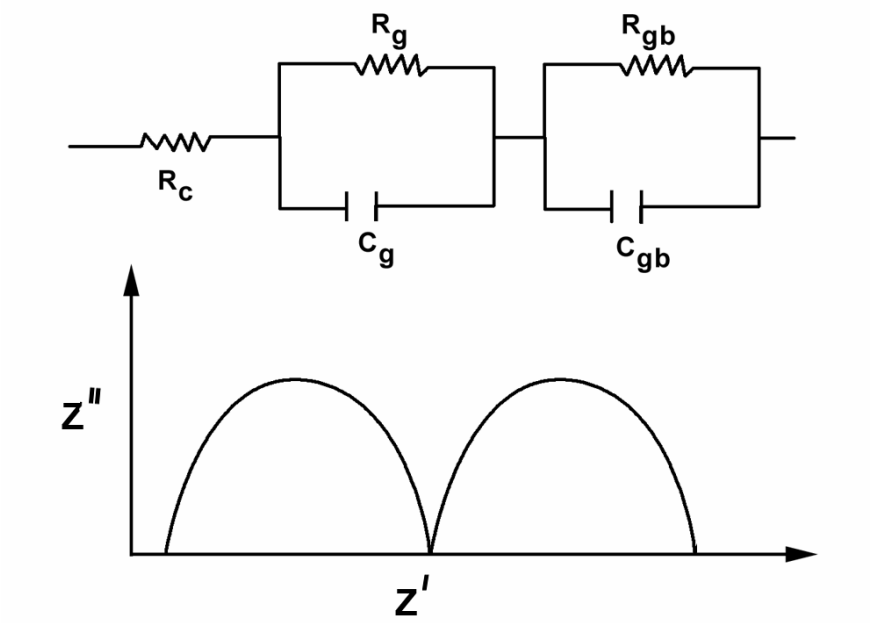

Figure 5. Schematic equivalent circuit and ac impedance response of a bulk YSZ.

Typical experimental impedance measurement data for the 4 wt% Al_2O_3 doped specimen at 700, 750, and 800°C in the frequency range of 0.1 to 10^6 Hz are shown in Figure 6. The impedance plot is depicted by a distorted semicircle originating from a non-zero origin on the Z' axis. The temperature increase shrinks the diameter of the distorted circle, illustrating that the specimen becomes less resistive. The resistance value as determined from the diameter of the distorted semicircle on the Z' axis is also approximately equal to the dc resistance measured by a multimeter (also shown in Figure 6). The impedance plot of the 10 wt% Al_2O_3 specimen at 850°C (Figure 7) shows three resistance parameters, R_1, R_2, and R_{total}. The R_1 parameter corresponds to the contact resistance whereas R_2-R_1 parameter is the grain resistance. The grain boundary resistance is equal to R_{Total}-R_2. These resistances (R_2-R_1 and R_{Total}-R_2) were normalized with specimen geometry (thickness and cross sectional area) to obtain corresponding resistivities (ρ) or conductivities ($\sigma = \frac{1}{\rho}$). It should be noted that R_2-R_1 is the diameter of a small semicircle barely discernible (see insert in Figure 7), implying that the grain possesses both capacitive and resistive elements. The grain boundary of the specimen is characterized by much larger resistive and capacitive elements.

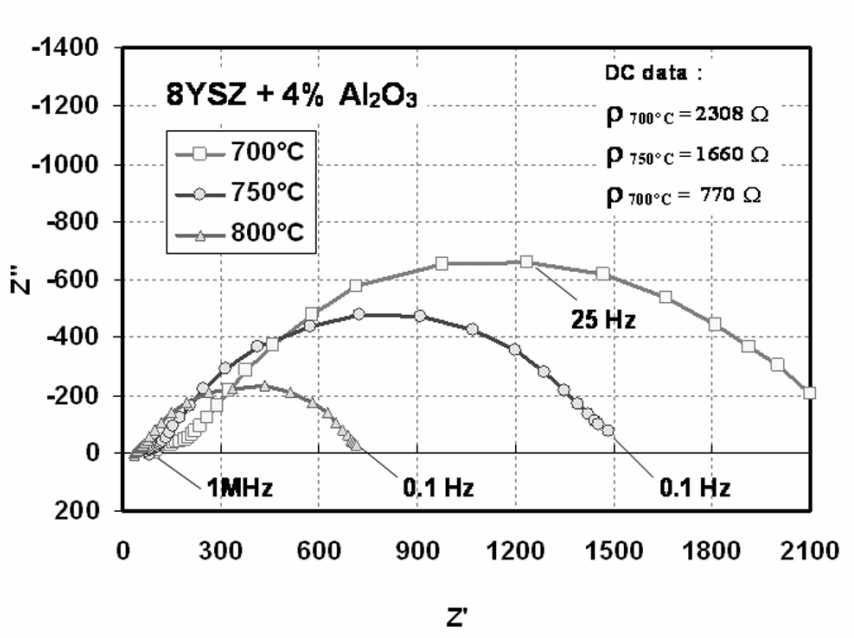

Figure 6. AC impedance measurement plots at 700 to 800°C for 8YSZ + 4% Al_2O_3.

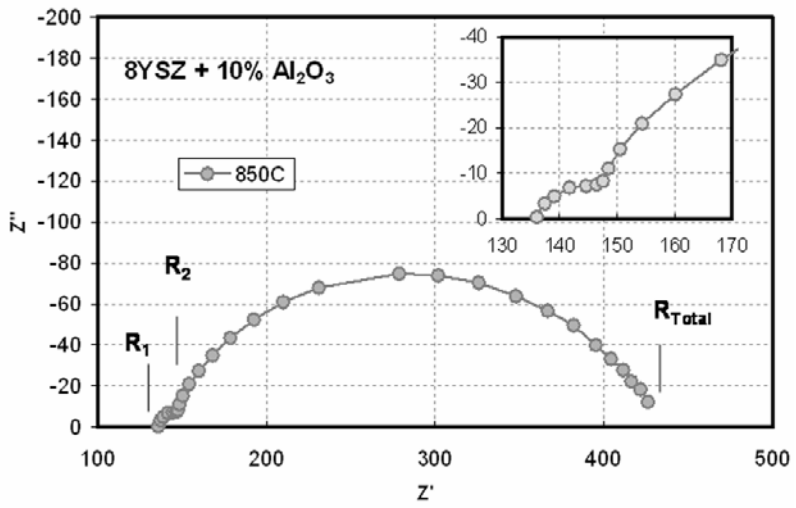

Figure 7. Determination of resistivities of grain and grain boundary from an ac impedance plot: R_1 is the interface resistance; the grain resistance $R_{grain} = R_2 - R_1$, and the grain boundary resistance $R_{G.B} = R_{Tot} - R_2$.

The Arrhenius plots of the grain and grain boundary conductivities of the undoped, 4 wt% Al_2O_3 and 20 wt% Al_2O_3 are shown in Figure 8. It should be noted that the grain conductivity is over an order of magnitude greater than the grain boundary conductivity. The difference between the grain and grain boundary conductivities is less than the value reported for the 8YSZ by Guo, et al.[18] The bulk, total conductivity comprised of grain and grain boundary contributions is shown in Figure 9. Again in this case the data sets are clustered and it appears that the doping concentration up to 20 wt% Al_2O_3 has decreased the conductivity; however, the dopant appears to have a minor influence.

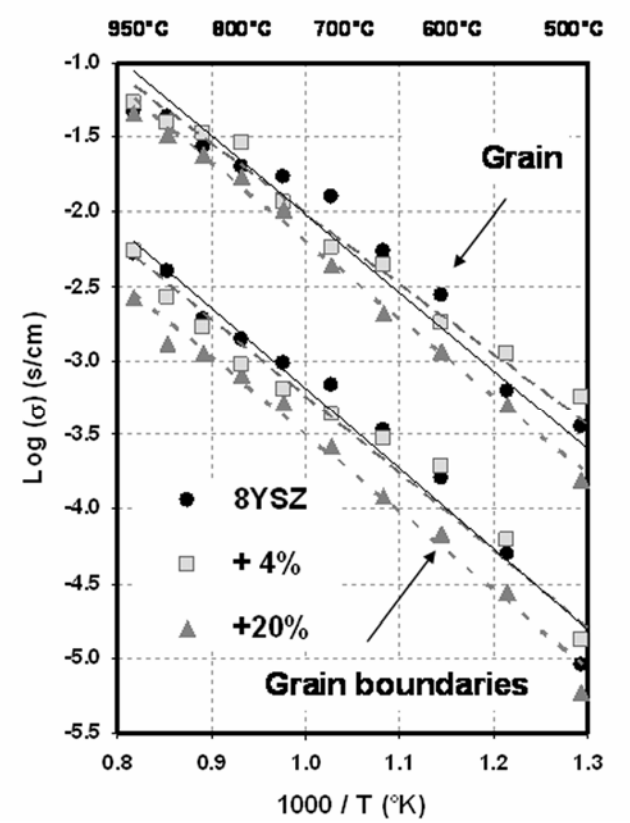

Figure 8. Conductivity shown as log(σ) vs. 1000/T for 8YSZ and 8YSZ + 4 to 20% alumina.

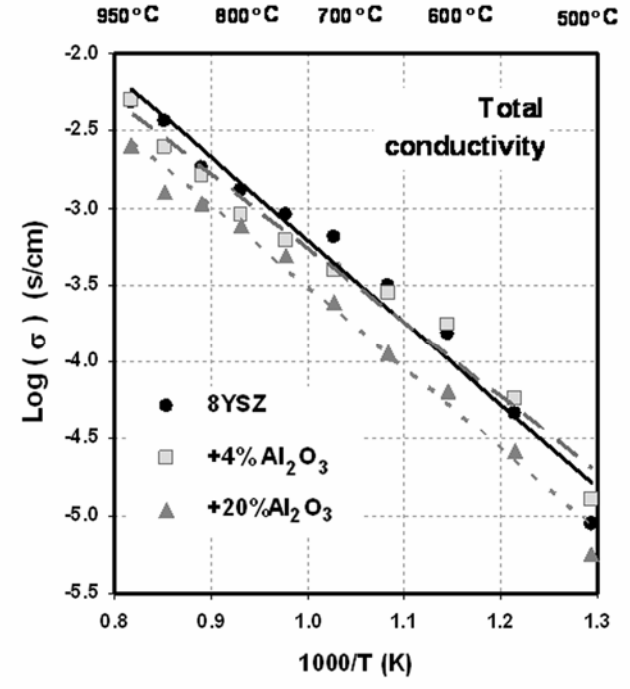

Figure 9. Arrhenius plots: total conductivity shown as log(σ) vs. 1000/T for 8YSZ and 8YSZ + 4 to 20% alumina.

The observations on the electrical conductivity of the doped specimens of this investigation parallel the observations made by Mori, et al.[15] and Feighery and Irvine.[16] Mori, et al.[15] reported that the bulk conductivity of 8YSZ doped with Al_2O_3 increased slightly with increasing Al_2O_3 up to 1 wt%. Furthermore, they reported that the conductivity of 20 wt% Al_2O_3 was around 0.1 S cm^{-1} at 1000°C, about 65% of that of the undoped 8YSZ. Mori, et al.[15] had doped the 8YSZ with up to 30 wt% of Al_2O_3 without observing a major drop in ionic conductivity. Similarly, Feighery and Irvine[16] had also doped 8YSZ with Al_2O_3 up to 24 wt%; however, they reported that 10 wt% Al_2O_3 can be introduced to the 8YSZ without a significant reduction in the ionic conductivity. Further additions of Al_2O_3 caused a rapid reduction in the conductivity, which was rationalized on the basis of the presence of a large volume fraction of insulating Al_2O_3 phase. Neither Mori, et al.[15] nor Feighery and Irvine[16] analyzed contributions of grain and grain boundaries independently on the total, bulk conductivity in these heavily-doped YSZ-Al_2O_3 composites.

Since there is a major reduction in the ionically conducting (active) phase in these 8YSZ-Al_2O_3 composites, a normalized plot of ionic conductivity versus Al_2O_3 may be useful to delineate the effect of Al_2O_3 additions. Normalized conductivity (conductivity of a composite/volume fraction of active phase) in S cm^{-1} of grain, grain boundary, and total conductivities is shown in Figure 10. The normalized grain conductivity shows an enhancement reaching a peak around 15 wt% of Al_2O_3. The conductivity enhancement is approximately 30%. The normalized grain boundary conductivity appears to increase initially up to about 4 wt% and then it gradually decreases. The grain boundary conductivity is lower than the grain conductivity by a factor of 10 to 15. The bulk, total conductivity shows a trend similar to the grain boundary, as it is the dominating factor.

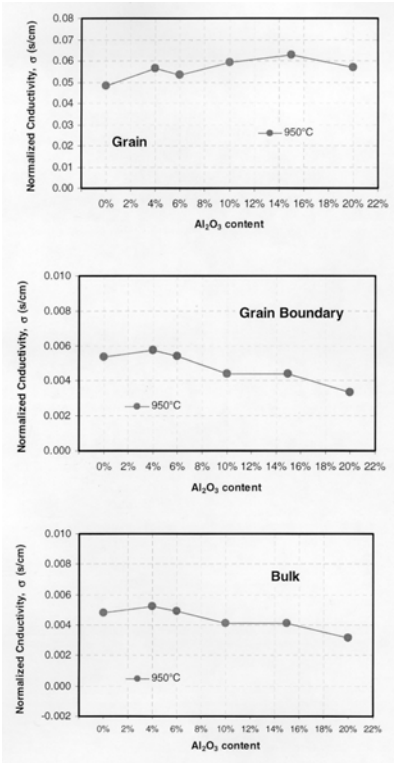

Figure 10. Normalized conductivity vs. Al_2O_3 content.

It is of significant relevance to review the effect of inert dopant on the conductivity of an ionically conducting matrix. A general trend on the effect of dopant particles on the ionic conductivity of composites is shown in Figure 11. With the addition of dopant particles, the ionic conductivity of composites increases and reaches a peak around 20 vol% of the insulating dopant. Further increases of the dopant decreases the conductivity as it impedes the transport of charged species. A steady-state percolation

of the conducting ion occurs around 20 vol% of the insulating dopant phase leading to an optimum conductivity. The percolation threshold may vary depending upon the matrix dopant chemistries, particle sizes, and processing parameters. The particle size of the dopant has a major influence on the conductivity, which has been reported in earlier publications.[6-8]

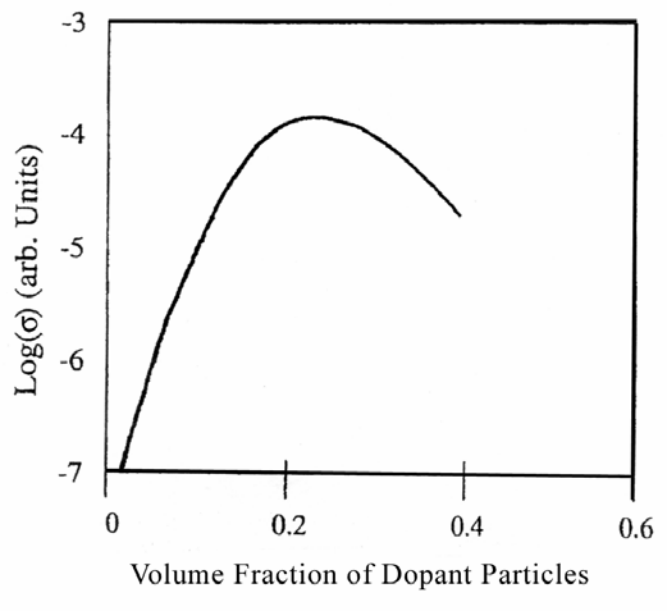

Figure 11. Low temperature ionic conductivity of ionically conducting matrix reinforced with insulating particles.

The conductivity data of this investigation does not show a trend characteristic of composite ionic conductors as depicted by Figure 11 because of (1) widely different contributions of the grain and grain boundaries to the bulk conductivity of the host material;(2) dissolution, precipitation and grain growth of the dopant phase; and (3) antagonistic influences of the dopant on conductivity. The contributions of grain and grain boundary to total bulk conductivity have been discussed earlier. The dissolution and precipitation of the dopant phase is evident from the microstructures as presented in Figure 2. Guo and Maier[17] investigated YSZ doped with 0.4 mol% Al_2O_3 in the temperature range of 200 to 500°C. Since no Al_2O_3 particles were observed in their SEM images, it was suggested that 0.4 mol% was within the solubility limit. The contribution of Al_2O_3 doping to the grain conductivity was insignificant; however, it drastically decreased the grain boundary conductivity almost by a factor of six. In this investigation, the concentration of Al_2O_3 is much greater and the presence of Al_2O_3 particles primarily at the grain boundaries leads to the formation of space charge regions, which are known to assist transport of charged specie, as in other composite ionic conductors. At the same time, Al_2O_3 particles at larger volume fractions may also impede the transport of the charged specie. Both of these influences on conductivity appear to counteract each other in the specimens investigated in this study. It is known from the work of Guo and Maier[17] that a small amount of Al_2O_3 is detrimental to conductivity. The addition of an excess of Al_2O_3, which is physically present in the structure, should also hinder transport of the conducting ions. These two factors, therefore, should lead to a rapid drop in the conductivity with Al_2O_3 additions. However, experimental evidence from this investigation and also those of Mori, et al.[15] and Feighery[16] are contradictory; thus, one is led to conclude that space charge regions at the YSZ-Al_2O_3 phase boundaries are created which augment the transport of oxygen ions, but a distinct conductivity peak is not observed. Thus, it is suggested that the dopant, Al_2O_3, imparts antagonistic influences to the total conductivity.

SUMMARY AND CONCLUSIONS

This paper investigated the effects of nanosize Al_2O_3 doping on conductivity of 8 mol% yttria stabilized zirconia. The Al_2O_3 doping concentration was varied from 0 to 20 wt% and the specimens were characterized by SEM, XRD, and impedance spectroscopy. The significant conclusions of the investigation are summarized as follows.

1. The composite specimens of this investigation were truly heterogeneous as evidenced by SEM micrographs and XRD data. The solid solubility between the YSZ and Al_2O_3 was minimal, as no significant change in the d-spacings occurred.

2. Initially there was a grain growth with the addition of Al_2O_3 up to about 6 wt%. The grain size increased from 4 to 6 μm and the grain boundaries became sharper. With further addition of Al_2O_3, the grain size decreased to 1.6 μm for 20 wt. Al_2O_3.

3. The conductivity data of the bulk specimen obtained from the ac measurement revealed a minor influence on the total, bulk conductivity due to the addition of Al_2O_3. The conductivity remained relatively flat as the Al_2O_3 content was increased. Both grain and grain boundary conductivities were characterized and their contributions were
discussed.

4. The conductivity variation was explained on the basis of antagonistic influences of Al_2O_3 doping. The doping leads to the creation of space charge regions in the vicinity of YSZ-Al_2O_3 boundaries, which should enhance transport of oxygen ions and thus conductivity. The presence of Al_2O_3 may also lead to a blocking effect suppressing conductivity. The net effect of the two antagonist influences is small and reflected by a relatively flat conductivity as the concentration of Al_2O_3 was increased.

ACKNOWLEDGMENT

Three of the authors, Binod Kumar, Christina Chen, and Chakrapani Varanasi, gratefully acknowledge the financial support by the Air Force Research Laboratory, Propulsion Directorate, under Contract No. F33615-02-D-2299.

REFERENCES

1. X. Guo and Y. Ding, *J. Electrochem. Soc.* 151 (1), J1-J7 (2004).
2. C.C. Liang, *J. Electrochem. Soc.* 120, 1289 (1973).
3. K. Shahi and J.B. Wagner, *Solid State Ionics* 3/4, 295 (1981).
4. T. Jow and J.B. Wagner, *J. Electrochem. Soc.* 126, 1963 (1979).
5. K. Hariharan and J. Maier, *J. Electrochem. Soc.* 142 (10), 3469 (1995).
6. B. Kumar, S.J. Rodrigues, and L.G. Scanlon, *J. Electrochem. Soc.* 148 (10), A1191 (2001).
7. R.C. Agrawal and R.K. Gupta, *J. Mat. Sci.* 34, 1131 (1999).
8. A. Mikrajuddin, G. Shi, and K. Okuyama, *J. Electrochem. Soc.* 147(8), 3157-3165 (2000).
9. P. Knauth, *J. Electroceramics* 5(2), 111-125 (2000).
10. B. Kumar and L.G. Scanlon, *J. Power Sources* 52, 261 (1994).
11. K.C. Radford and R.J. Bratton, *J. Mat. Sci.* 14, 66-69 (1979).
12. M.J. Verkerk, A.J.A. Winnubst, and A.J. Burggraaf, *J. Mat. Sci.* (17), 3113-3122 (1982).
13. E.P. Butler and J. Drennan, *J. Amer. Ceram. Soc.* 65 (10), 474-478 (1982).
14. M. Miyayama, H. Yanagida, and A. Asada, *Am. Ceram. Soc. Bull.* 64 (1), 660-664 (1985).
15. M. Mori, T. Abe, H. Itoh, O. Yamamoto, Y. Takeda, and T. Kawahara, *Solid State Ionics* 74, 157-164 (1994).
16. A.J. Feighery and J.T.S. Irvine, *Solid State Ionics* 121, 209-216 (1999).
17. X. Guo and J. Maier, *J. Electrochem. Soc.* 148 (3), E121-126 (2001).
18. X. Guo, W. Sigle, J. Fleig, and J. Maier, *Solid State Ionics* 154-155, 555-561 (2002).

Appendix C

Electrical Conductivity Enhancement in Heterogeneously Doped Scandia Stabilized Zirconia

Chakrapani Varanasi, Chetan Juneja, Christina Chen, Binod Kumar
University of Dayton Research Institute

Abstract: Composites of 6 mol% Scandia stabilized zirconia materials (6ScSZ) and nanosize Al_2O_3 powder (0 to 30 wt%) were prepared and characterized for electrical conductivity by the ac impedance method at various temperatures ranging from 300 to 950^{o}C. All the composites characterized showed improved conductivity at higher temperatures compared to the undoped ScSZ. An average conductivity of 0.12 S/cm was measured at 850^{o}C for 6 ScSZ + 30 wt% Al_2O_3 composite samples, an increase in conductivity up to 20% compared to the undoped 6 ScSZ specimen at this temperature. Microstructural evaluation using scanning electron microscopy revealed that the ScSZ grain size was relatively unchanged up to 10 wt% of Al_2O_3 additions. However, the grain size was reduced in samples with higher (20 and 30 wt%) additions of Al_2O_3. Small grain size, reduced quantity of the 6ScSZ material (only 70%), and improved conductivity makes these ScSZ + 30 wt% Al_2O_3 composites very attractive as electrolyte materials in view of their collective mechanical and electrical properties and cost requirements. The observed increase in conductivity values with the additions of an insulating Al_2O_3 phase is explained in light of the space charge regions at the 6 ScSZ-Al_2O_3 grain boundaries.

Introduction: A superior alternative to the developed tubular solid oxide fuel cell (SOFC) is a planar design. The planar design yields an enhanced stack performance and much higher power density as compared to the tubular design. The high power density is critical to reduced costs, as the amount of required material per KW is minimized. Furthermore, the planar design can use low-cost fabrication methods such as screen printing and tape casting. However, electrical conductivity, mechanical strength, thermal robustness, durable sealant, and fracture initiation during thermal cycling are some of the technical issues that limit development and commercialization of the planar design.

Scandia stabilized zirconia (ScSZ) materials are known to exhibit higher conductivity as compared to the state-of-the-art yttria stabilized zirconia (YSZ) materials. The conductivity enhancement in the ScSZ material is attributed to the minimal difference in ionic radii of the host Zr and dopant Sc [1]. The activation energy for the transport of oxygen ions in the ScSZ materials is also reduced as compared to the

YSZ material [1]. There is a strong interest in the ScSZ materials, primarily motivated by improved conductivity, and a number of groups, specifically in Japan, are pursuing active research efforts [2-4].

A number of different approaches can be employed to enhance conductivity of the bulk electrolyte. The aforementioned YSZ and ScSZ materials were developed by the technique of homogeneous doping in which the host zirconium sites are replaced by yttrium and scandium sites. An alternate route to enhance bulk conductivity of stabilized zirconia is to employ a heterogeneous dopant. These heterogeneous dopants are insoluble in host YSZ or ScSZ and remain a physically distinct phase of the bulk structure. For a number of ionic conductors, it has been demonstrated that the existence of an inert, heterogeneous dielectric phase in a conducting matrix can raise the ionic conductivity by orders of magnitude [5-11].

In a pioneering work, Liang [5] investigated polycrystalline lithium iodide doped with aluminum oxide and reported that lithium iodide doped with 35 to 45 mol% aluminum oxide exhibited conductivity on the order of 10^{-5} S cm^{-1} at 25°C, about three orders of magnitude higher than that of the LiI conductivity. However, no significant amount of aluminum oxide was determined to be soluble in LiI; thus, the conductivity enhancement could not be explained by the classical doping mechanism and creation of Schottky defects such as in the LiI-CaF_2 system. Subsequently, a number of investigations have reported enhanced conductivity of silver in the AgI-Al_2O_3 system [6], copper in the CuCl-Al_2O_3 system [7], fluorine in the PbF_2-SiO_2 and PbF_2-Al_2O_3 systems [8], and lithium in polymer-ceramic composite electrolytes [9]. Four review papers [10-13] also document the developmental history and general characteristics of these fast ionic conductors. Analyses of these reviews point out that a new conduction mechanism evolves which augments the bulk conductivity of single-phase ionic conductors. The new conduction mechanism uses interfacial and/or space charge regions between the two primary components. The interfacial or space charge regions are formed because of the creation of charged vacancies and adsorption/desorption of ions. In effect, these regions are electrically active, which influences the transport of conducting ions.

A recent investigation of heterogeneously doped YSZ materials with nanosize Al_2O_3 revealed that the Al_2O_3 dopant may lead to an enhancement and/or blockage of the conducting oxygen ions [14]. These effects are antagonistic and in effect may neutralize each other. The net result of Al_2O_3 doping in the aforementioned investigation [14] was small and conductivity variation revealed a minor influence on the

total bulk conductivity. The objective of the present study was to further elucidate the composite effect in heterogeneously doped 6 mol% scandium doped zirconium oxide (6 ScSZ) materials. The composites may also provide improved fracture toughness, mechanical strength, and reduced cost. These attributes may lead to an electrolyte material that may satisfy requirements of the aforementioned planar design SOFC.

Experimental: ScSZ materials used were obtained from Tosoh Corporation* and the nanosize Al_2O_3 powder was obtained from Nanophase Technologies Corporation+. The amount of Scandia used in the ScSZ as per the manufacturer's specification is 6 mol% (6 ScSZ). Appropriate amounts of 6 ScSZ powder and Al_2O_3 powders were weighed and then mixed in a mortar and pestle to prepare 6 ScSZ + Al_2O_3 composites containing 0, 10, 20, and 30 wt% Al_2O_3. Powder batch compositions were pressed in a cold isostatic press at 3 ton/cm^2 pressure using collapsible tygon tubes to obtain specimens with dimensions of 0.6 mm diameter and approximately 2 cm long. The cylindrical shaped samples were heated at a rate of 20^{o}C/min to 1520^{o}C in air and kept at this temperature for 4 hours and then cooled at a rate of 20^{o}C/min to 950^{o}C. Subsequently, they were soaked at 950°C for 1 hour before they were finally allowed to cool to room temperature by shutting the power off to the furnace. This procedure was followed to minimize the Al_2O_3 particle coarsening during heating which was an issue during an earlier investigation [14]. Several discs of 0.5 mm thickness were cut from these cylindrical specimens using a diamond saw.

The specimen density was determined using the Archimedes principle. One set of the discs were polished, thermally etched, and carbon coated by thermal evaporation for microstructural analysis using a Leica FE 960 scanning electron microscope (SEM). Similarly, polished specimens were also used for the hardness measurement using a Vickers hardness tester. Another set of discs was used to obtain x-ray diffraction (XRD) data using a Rigaku Rotaflex RV-200BH x-ray diffractometer operated at 40 KV, 150 mA current with a copper target.

AC impedance spectroscopy measurements in the 0.1 to 10^6 Hz frequency range were conducted on three different sets of discs of each composition using a Solatron 1260 impedance analyzer with 1287 electrochemical interface. The ac impedance data were obtained at several temperatures ranging from 300 to 950^{o}C. For the electrical conductivity measurements, the discs were coated on both sides with Pt paint and then fired in an ambient atmosphere furnace at 1000^{o}C for one hour and subsequently furnace cooled.

* Tosoh Corporation, 4560 Kaisei-Cho, Shinnanyo-shi, Yamaguchi-Ken 746-8501, Japan.
+ Nanophase Technologies Corporation, 8205 S. Cass Ave. #105, Darien, IL 60561.

The fixture used in the present study consists of a machined glass ceramic macor screw and socket design that can be tightened to provide intimate contact between the electrodes and the specimen. The fixture containing the specimen is inserted into a tube furnace and the data collected at several temperatures after stabilizing for 15 minutes at each temperature. The thermocouple was placed closest to the fixture in each measurement to ensure accuracy of the temperature measurement. A single crystal YSZ specimen was also characterized to establish the baseline for the ac impedance measurement. The same fixture and similar experimental procedure was used for the three sets of specimens to determine measurement errors and establish limits.

Results and Discussion

Table 1 presents calculated and measured densities of specimens doped with different concentrations of Al_2O_3. Since the density of Al_2O_3, 3.97 g/cm^3, is lower than the density of the stabilized zirconia, the densities of all doped specimens decrease with increasing concentration of the dopant. Also as expected, the measured densities are lower than the theoretical densities. However, with the increase of Al_2O_3 concentration, the difference between the measured density and the theoretical density increased. This observation is consistent with the earlier findings with YSZ-Al_2O_3 composites [14]. The Al_2O_3 particles inhibit the sintering and grain growth of the 6ScSZ grains and perhaps trap some porosity in the microstructure, thereby reducing the density. However, since the density greater than 94% of the theoretical values is achieved even with 30 wt% of Al_2O_3, it was not considered to be a significant issue for further investigation.

As mentioned earlier, the fixture used in the present study requires the tightening of a macor screw to obtain good electrical contact, and so the samples are required to have good strength and undergo repeated measurements without developing cracks. The Vickers hardness obtained from the polished samples varied from 1337 to 1398 without a specific trend. It is interesting to note that no hardness degradation was measured even after 30% of 6 ScSZ was replaced with Al_2O_3. All the composite samples in this study exhibited high mechanical integrity so that repeated measurements on a single, thin ($\underset{\sim}{}$ 0.05 cm) specimen can be made without fracturing it.

Figure 1 (a-d) shows the XRD patterns obtained from the sintered specimen. It is noted that in the undoped 6 ScSZ specimen, both tetragonal and cubic phases are present, Figure 1(d). The most intense XRD peak corresponding to these two phases is present at around $2\theta = 30°$. The addition of nanosize Al_2O_3 leads to the formation of the monoclinic phase shown by an arrow in the diffraction pattern of the composite containing 30 wt% Al_2O_3, Figure 1(d). The observations relating to the existence of crystalline phases in the undoped specimen, i.e., presence of both tetragonal and cubic phases, are consistent with earlier reports [1,3].

The phase diagram in the ZrO_2-Sc_2O_3 system [15] also predicts the existence of a monoclinic phase along the tetragonal and cubic phases if the specimen is cooled under equilibrium conditions. However, the undoped ScSZ specimen processed under similar conditions does not show the presence of the monoclinic phase. Therefore, the existence of the monoclinic phase in the Al_2O_3 doped specimens must be related to the presence of Al_2O_3 and perhaps the existence of a ScSZ-Al_2O_3 solid solution. The ionic radii of Zr^{4+}, Sc^{4+}, and Al^{3+} are 0.80, 0.81, and 0.50 Å and considering the large difference in the ionic radii of Zr^{4+}/Sc^{4+} and Al^{3+} sites, only a very limited solid solubility of Al_2O_3 in the ScSZ can be expected.

With the increased additions, the intensity of peaks corresponding to Al_2O_3 phase is increased and no additional extraneous peaks were observed indicating that no chemical interactions with the matrix have taken place. Also, no noticeable peak shift was observed which indicates that the solubility of Al_2O_3 in ScSZ is minimal due to a large difference in the ionic radii. As noted earlier, up to 1 wt% Al_2O_3 can dissolve in YSZ when maintained at 1500°C for 24 hours [16]. Since in the present study the specimens were kept at 1500°C for a short period (only 4 hours), the solubility is expected to be lower.

Figure 2 shows the scanning electron micrographs of the specimens doped with different concentrations of Al_2O_3. Dense microstructure with some porosity can be observed in all the samples. While some of the Al_2O_3 particles (dark areas) can be observed at the grain boundaries in the composite samples, occasionally some particles were also entrapped inside the ScSZ grains. A reduction in grain size by a factor of 2 is observed in 6ScSZ with 30% Al_2O_3 composites as compared to undoped 6ScSZ samples. The variation in ScSZ grain size with the Al_2O_3 additions is shown in Figure 3. Although nanosize Al_2O_3 was used, a wide size distribution of Al_2O_3 particles is observed in 6ScSZ with 20% and 30% Al_2O_3 composite specimens, Figure 2 (c,d). The average grain size of Al_2O_3 is about one micron in these

specimens [2 (c,d) micrographs]. In higher concentrations of Al_2O_3 doped samples (20% and 30% doping level), the coarsening of the particles is evident at the triple points. Dissolution and re-precipitation of Al_2O_3, including particle coarsening is attributed to the observed microstructures. The ScSZ grain growth was inhibited at higher Al_2O_3 doping levels, resulting in small grain size. It may also be possible to modify the heat treatments to obtain fine grain size of Al_2O_3 in these composites.

AC impedance plots of one 6ScSZ+30% Al_2O_3 specimen obtained at several temperatures (300 to 950ºC) are shown in Figure 4 (a-f). It can be seen that the appearance shown by the semicircles and their intersections with real axis (Z') change with the temperature of the measurement. The intercept of the first semicircle closest to the origin in all the plots is due to the contact resistance arising at the electrolyte-electrode interface. There are three different regions in the 300° temperature measurement plot. The first semicircle (marked 1) in Figure 4(a) from the left is due to the grain resistance, the second semicircle (marked 2) results from the grain boundary resistance and the third incomplete semicircle (marked 3) is due to the resistive capacitive component of the electrode-electrolyte interface. However, as the temperature of the measurement is increased, the capacitances of the grain boundary and grain become comparable and one of the semicircles (corresponding to the grain) disappears. Hence at high temperatures, the first semicircle is due to the combined grain and grain boundary electrical properties (resistance and capacitance) and the second semicircle is due to the electrode-electrolyte interface. This interpretation of the impedance spectra was used for all the data collected in this study.

Figure 5 (a-d) shows the impedance plots obtained from the samples with different amounts of Al_2O_3 additions at 850°C. It can be seen that all the curves show two semicircles and the diameter of the first semicircle diameter corresponds to the bulk resistance including grain and grain boundary and is reduced with increasing amounts of Al_2O_3, indicating that the bulk conductivity has increased. The second semicircle diameter that depicts electrical properties of the electrode-electrolyte interface varies from specimen to specimen in an inconsistent manner. Figure 6 (a-d) again shows the impedance plots of specimens containing various amounts of Al_2O_3 at 950°C. The trend is very similar to Figure 5 (a-d), in that the diameter of the first semicircle decreases with temperature and the second semicircle, showing an inconsistent trend. The bulk resistance of the specimen which is equivalent to the diameter of the first semicircle and obtained directly from Figures 5 and 6 are plotted in Figure 7 to show the trend of resistivity

reduction variation with the composition. It can be seen that at these temperatures, the resistance of the electrolytes is reduced by approximately 25% as Al_2O_3 concentration is increased.

Figure 8 (a-d) shows the mean conductivity of the samples measured at 800, 850, 900, and 950^{o}C as a function of Al_2O_3 concentration. Three specimens were characterized at each Al_2O_3 concentration. The conductivity values determined from these measurements, their mean and a solid line obtained by a regression analysis are also shown in Figure 8. It is noted that at all temperatures ranging from 800 to 950^{o}C the conductivity improves with the addition of Al_2O_3. The spread in conductivity values at a given temperature is considerable and may be a source of misinterpretation if not enough specimens are characterized at a given temperature. The spread in the measured conductivity values appears to increase with increasing concentration of Al_2O_3. This is expected because statistical distribution of the percolation path through which oxygen ions can be transported increases with higher Al_2O_3 concentration.

Figure 9 presents normalized conductivity; i.e., conductivity of the composite specimen divided by the volume of the active material (6 ScSZ). The conductivities at 900°C show greater enhancements as compared to 800°C as Al_2O_3 was increased. If the blocking effect of Al_2O_3 is taken into account, the conductivity data should exhibit a rapid drop with Al_2O_3 content. The conductivity enhancement as noted in Figure 9 must therefore be attributed to the formation of space charge regions which provide local electric fields and accelerates the transport of oxygen ions, thereby increasing the conductivity. The space charge mechanism assisted transport of conducting ions has been reported earlier [14].

Figure 10 shows Arrhenius plots of the conductivity of specimens in the 800 to 950°C temperature range. The activation energy for the transport of oxygen ions was determined to be in the range of 1.01 to 1.09 eV which is consistent with values reported in the literature. It is apparent that the conduction mechanism in these composites remains essentially the same.

Summary and Conclusions: This paper investigated the effects of nanosize Al_2O_3 doping on the conductivity of 6 mol% Scandia stabilized zirconia. The Al_2O_3 doping concentration was varied from 0 to 30 wt% and the specimens were characterized by SEM, XRD, and impedance spectroscopy. The significant conclusions of the investigation are summarized as follows:

1. The composite specimens of this investigation were truly heterogeneous as evidenced by SEM micrographs and XRD data. The solid solubility between the ScSZ and Al_2O_3 was minimal, as no significant change in the d-spacings occurred.
2. Initially, the grain size remained unaffected with the addition of Al_2O_3 up to about 5 wt%. With further addition of Al_2O_3, the grain size decreased to about 3 μm for 30 wt% Al_2O_3.
3. The conductivity data of the bulk specimen obtained from the ac measurement revealed enhancement of the total, bulk conductivity in the 800 to 950°C temperature range due to the addition of Al_2O_3. The conductivity increased as the Al_2O_3 content was increased up to 30 wt%. Both grain and grain boundary conductivities were characterized and at these temperatures contributions from these merge into a single semicircle in the impedance plot.
4. The conductivity variation was explained on the basis of antagonistic influences of Al_2O_3 doping. The doping leads to the creation of space charge regions in the vicinity of ScSZ-Al_2O_3 boundaries, which should enhance transport of oxygen ions and thus conductivity. The presence of Al_2O_3 may also lead to a blocking effect, which suppresses conductivity. The net result of the two antagonist influences is small but positive and reflected by an enhancement in conductivity as the concentration of Al_2O_3 was increased.
5. The activation energy for the transport of conducting ion oxygen was calculated to be around 1 eV and were found to be similar for undoped and doped specimens.

Acknowledgment

The authors gratefully acknowledge the financial support by the Air Force Research Laboratory, Propulsion Directorate, under Contract No. F33615-02-D-2299.

References:

1. Osamu Yamamoto, Yoshinori Arati, Yasuo Takeda, Nobuyuki Imanishi, Yasumobu Mizutani, Masayuki Kawai, and Yasuhisa Nakamura, *Solid State Ionics* 79, 137 (1995).
2. Y. Arachi, H. Sakai, O. Yamamoto, Y. Takeda, and N. Imanishai, *Solid State Ionics* 121, 133 (1999).
3. Masanori Hirano, Shinzi Watanabe, Etsuro Kato, Yasunobu Mizutani, Masayuki Kawai, and Yasuhisa Nakamura, *Solid State Ionics* 111, 161 (1998).
4. Y. Mizutani, M. Tamura, and M. Kawai, *Solid State Ionics* 72, 271 (1994).

5. C.C. Liang, *J. Electrochem. Soc.* 120, 1289 (1973).
6. K. Shahi and J.B. Wagner, *Solid State Ionics*, 3/4, 295 (1981).
7. T. Jow and J.B. Wagner, *J. Electrochem. Soc.* 126, 1963 (1979).
8. K. Hariharan and J. Maier, *J. Electrochem. Soc.* 142 (10), 3469 (1995).
9. B. Kumar, S.J. Rodrigues, and L.G. Scanlon, *J. Electrochem. Soc.* 148 (10), A1191 (2001).
10. R.C. Agrawal and R.K. Gupta, *J. Mat. Sci.* 34, 1131 (1999).
11. A. Mikrajuddin, G. Shi, and K. Okuyama, *J. Electrochem. Soc.* 147(8), 3157-3165 (2000).
12. P. Knauth, *J. Electroceramics* 5(2), 111-125 (2000).
13. B. Kumar and L.G. Scanlon, *J. Power Sources* 52, 261 (1994).
14. Binod Kumar, Christina Chen, Chakrapani Varanasi, and Joseph. P. Fellner, accepted for publication, *J. Power Sources* (2004).
15. F.M. Spiridonov, L.N. Popova, and R.Ya. Popilskii, *J. Solid State Chemistry* 2, 430 (1970).
16. Masanori Hirano, Takayuki Oda, Kenji Ukai, and Yasunobu Mizutani, *Solid State Ionics*, 158, 215 (2003).

Table 1. Calculated and Measured Density of the 6ScSZ and Al_2O_3 Composite Samples

Sample	Al_2O_3 (wt%)	Al_2O_3 (mol%)	Measured Density (g/cm^3)	Theoretical Density (g/cm^3)	% Of Theoretical Density
6SCSZ	0	0	5.82	5.87	99.15
6SCSZ +10% Al_2O_3	10	11.91	5.36	5.68	94.37
6SCSZ +20% Al_2O_3	20	23.3	5.205	5.49	94.81
6SCSZ +30% Al_2O_3	30	34.26	5.03	5.31	94.73

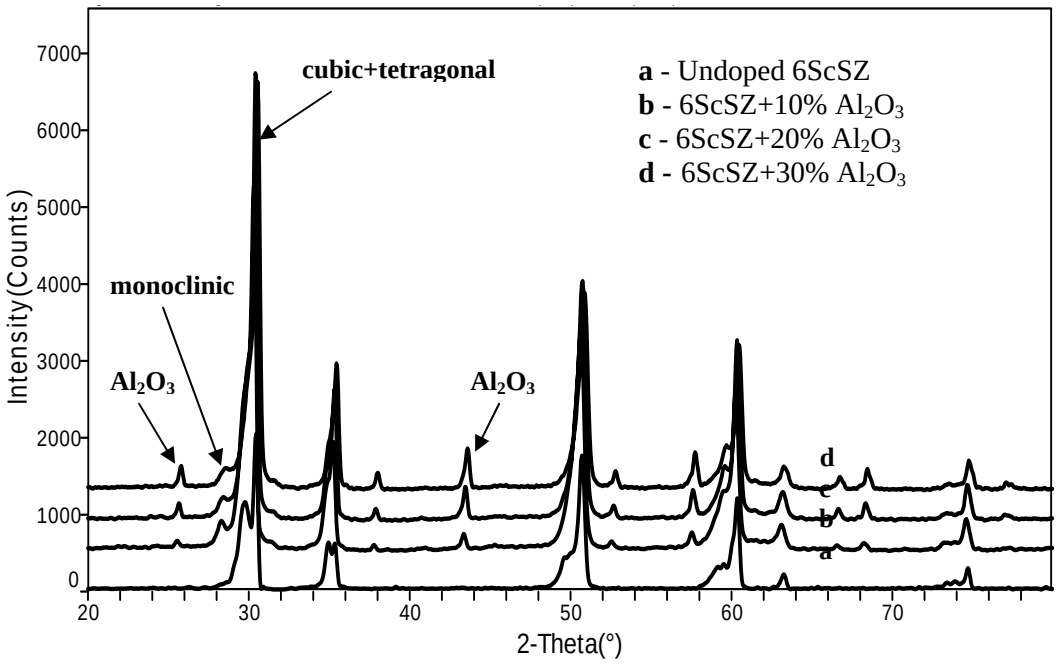

Figure 1. XRD patterns taken from the sintered pellets of 6ScSZ+ Al_2O_3 composites. (a) Undoped 6ScSZ, (b) 6ScSZ+10% Al_2O_3, (c) 6ScSZ+20% Al_2O_3, and (d) 6ScSZ+30% Al_2O_3.

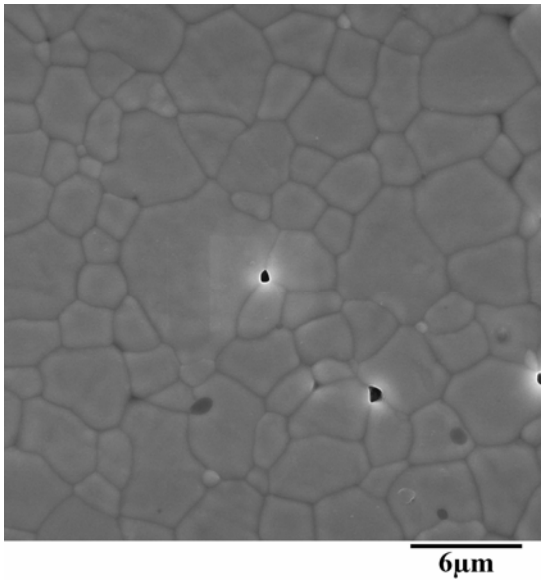

(a) Undoped 6ScSZ

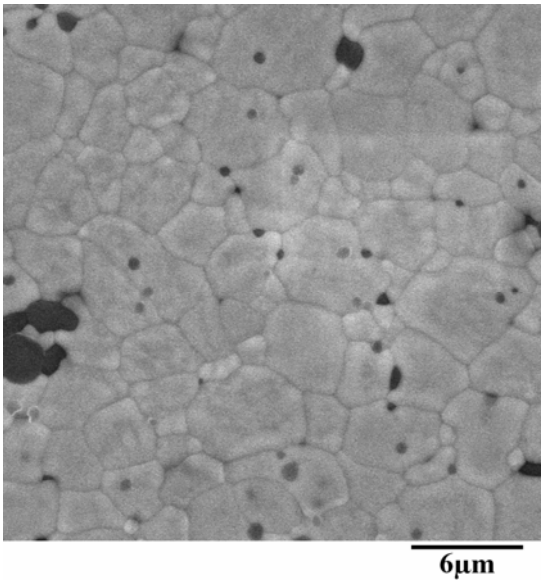

(b) 6ScSZ + 10% Al_2O_3

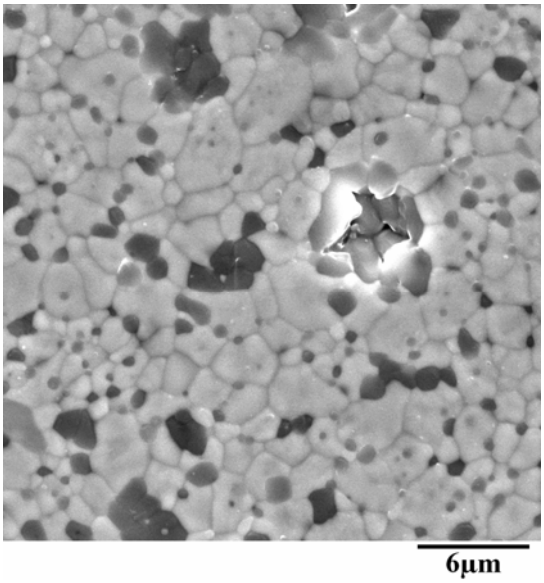

(c) 6ScSZ + 20 % Al_2O_3

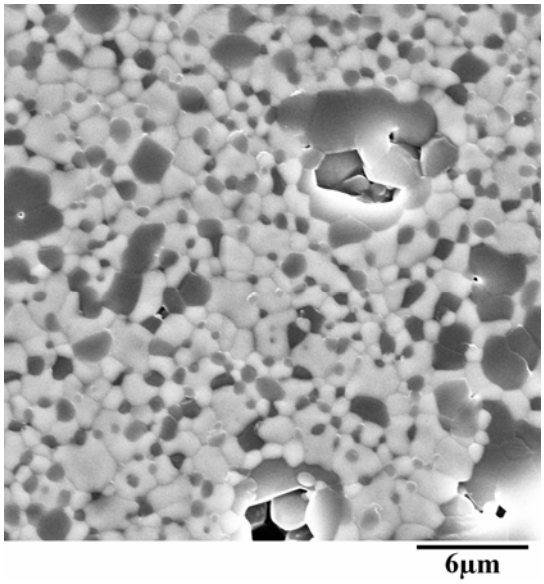

(d) 6ScSZ + 30% Al_2O_3

Figure 2. Scanning electron micrographs of polished and etched 6ScSZ+Al_2O_3 composites. (a) Undoped 6ScSZ, (b) 6ScSZ+10% Al_2O_3, (c) 6ScSZ+20% Al_2O_3, and (d) 6ScSZ+30% Al_2O_3. The dark contrast phase was is Al_2O_3 and the light color phase is ScSZ.

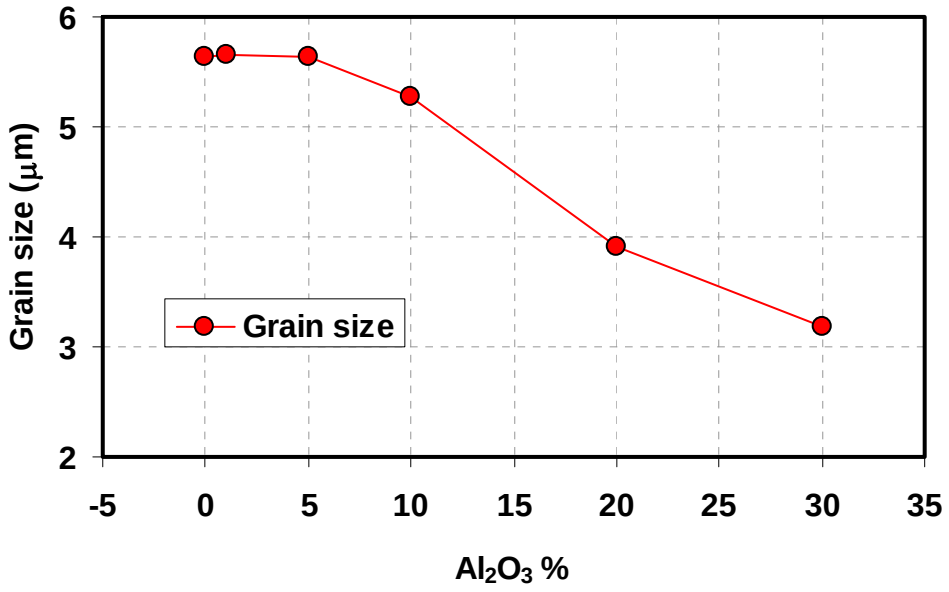

Figure 3. ScSZ grain size variation with Al_2O_3 additions in the sintered pellets.

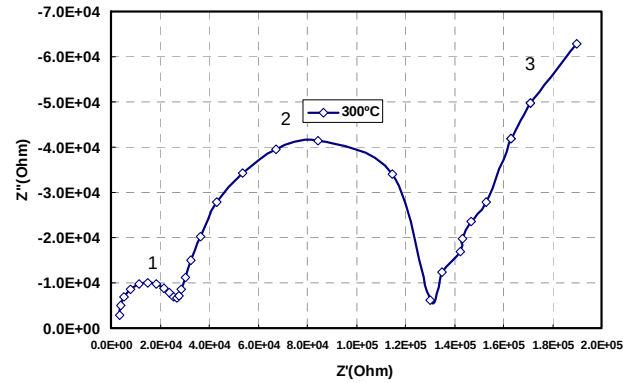

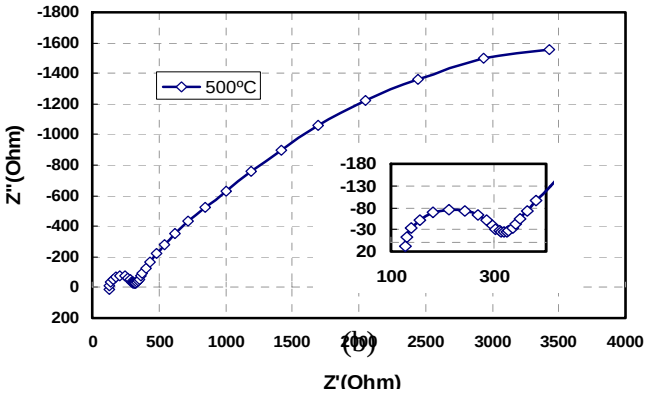

(b)

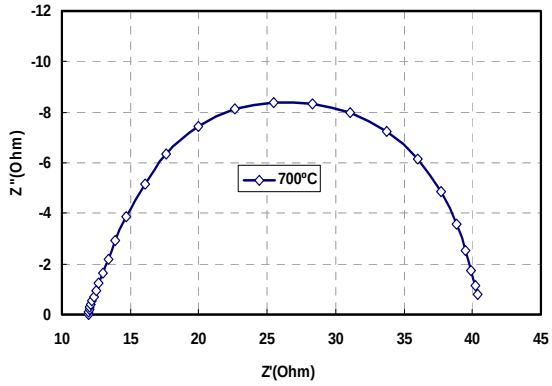

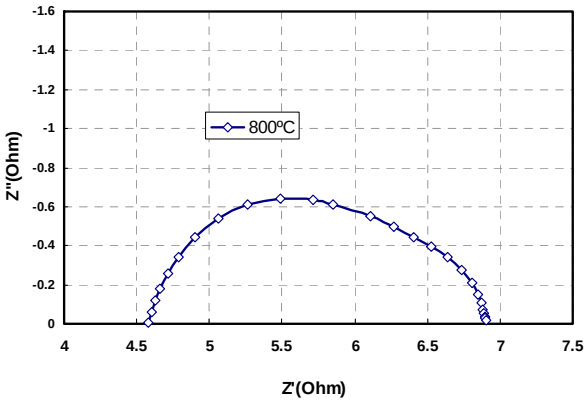

(c) (d)

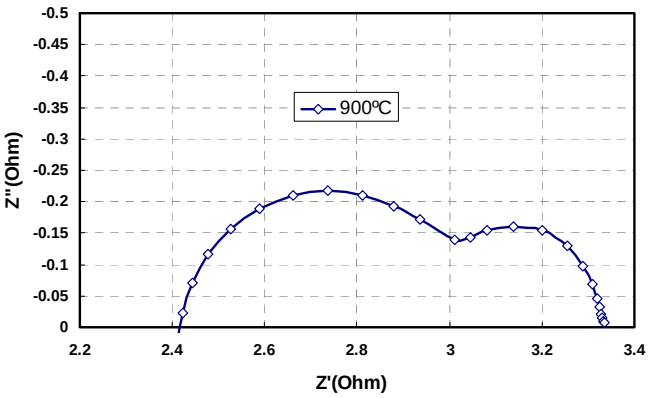

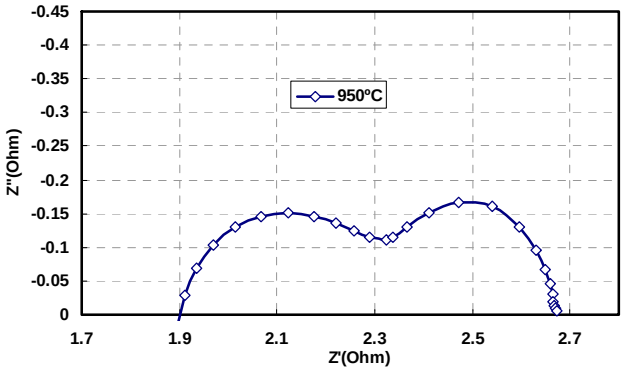

(e) (f)

Figure 4. Impedance plots of SSZ+30% Al_2O_3 at different temperatures ranging from 300 to 950ºC.

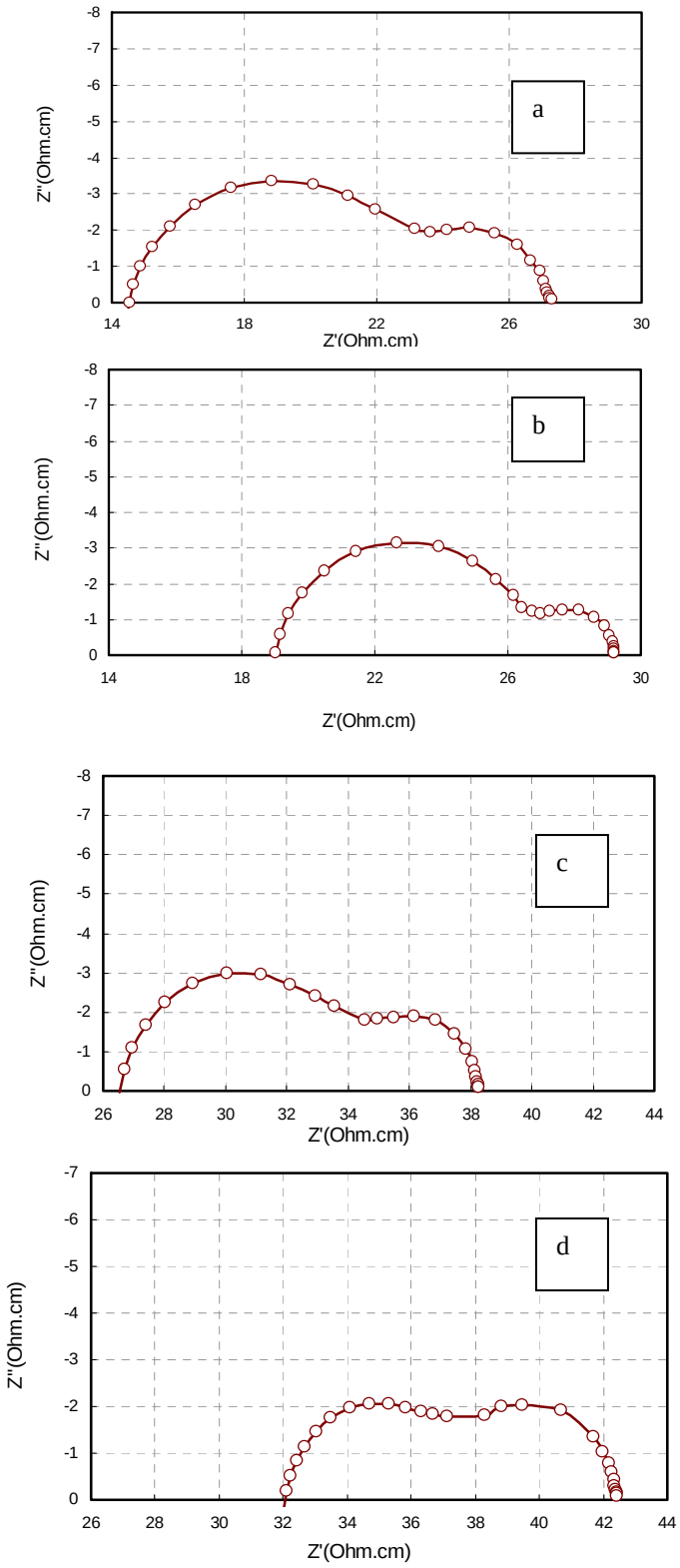

Figure 5. Impedance plots of (a) undoped 6ScSZ, (b) 6ScSZ+10% Al_2O_3, (c) 6ScSZ+20% Al_2O_3, (d) 6ScSZ+30% Al_2O_3 @ 850ºC.

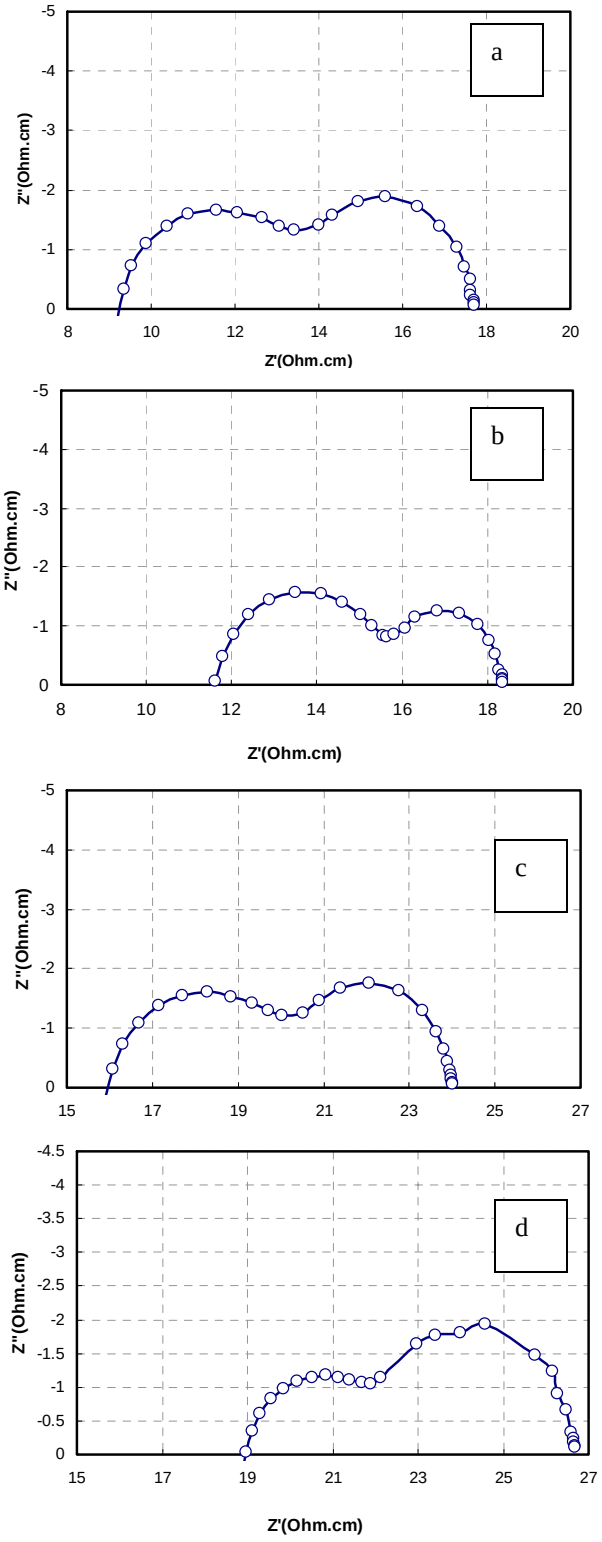

Figure 6. Impedance plots of (a) undoped 6ScSZ, (b) 6ScSZ+10% Al_2O_3, (c) 6ScSZ+20% Al_2O_3, (d) 6ScSZ+30% Al_2O_3 @ 950ºC.

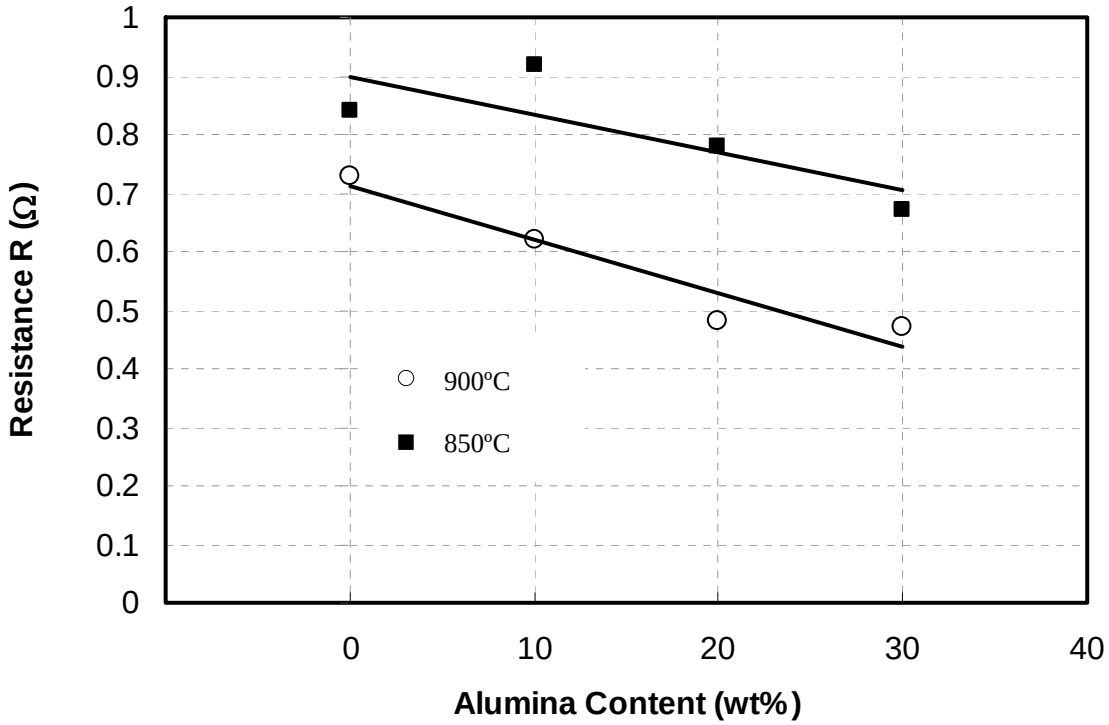

Figure 7. The diameter of the first circle in the Figures 5 and 6 that represent the resistance of the electrolyte is plotted as a function of the Al_2O_3 content.

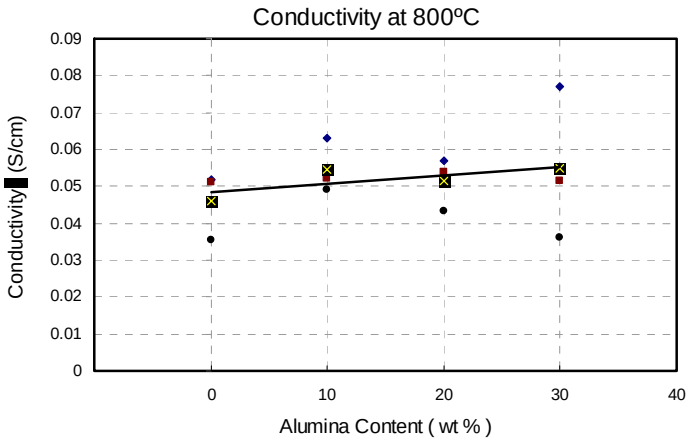

(a)

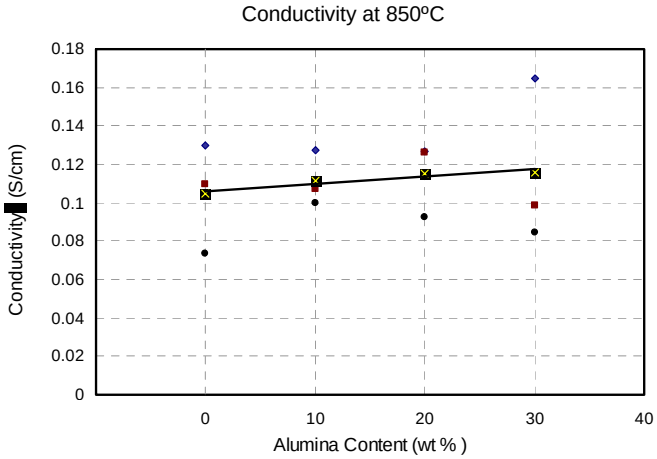

(b)

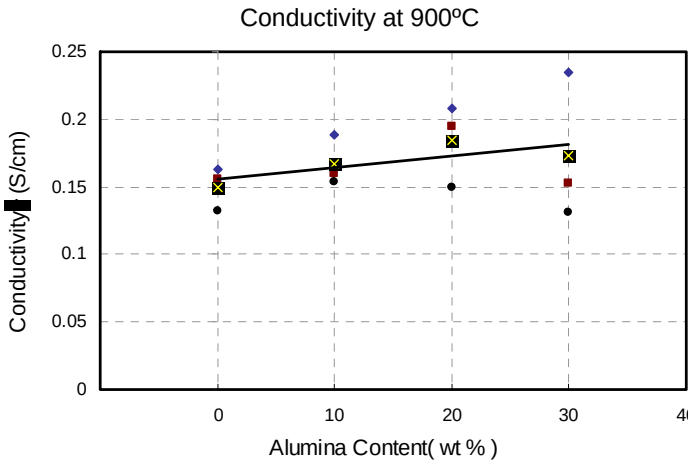

(c)

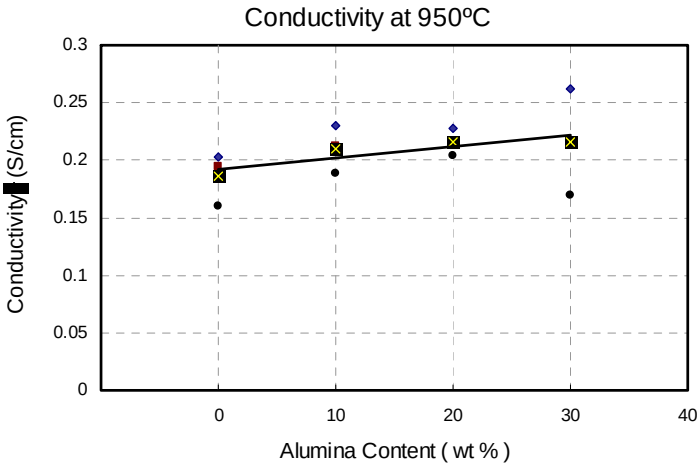

(c)

Figure 8. The mean conductivity as designated by of the samples measured at various temperatures (a) 800°C, (b) 850°C, (c) 900°C, (d) 950°C without correcting for the nonconducting Al_2O_3 phase.

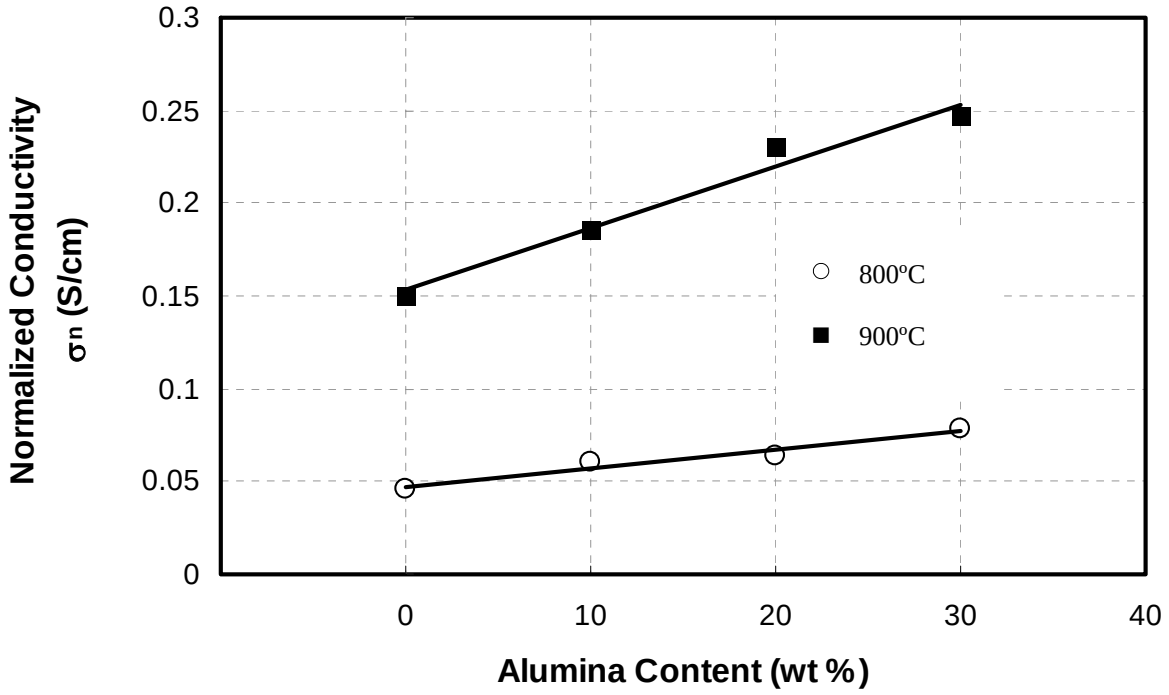

Figure 9. The average conductivity of the samples measured at 850 and 900°C after correcting for the nonconducting Al_2O_3 phase.

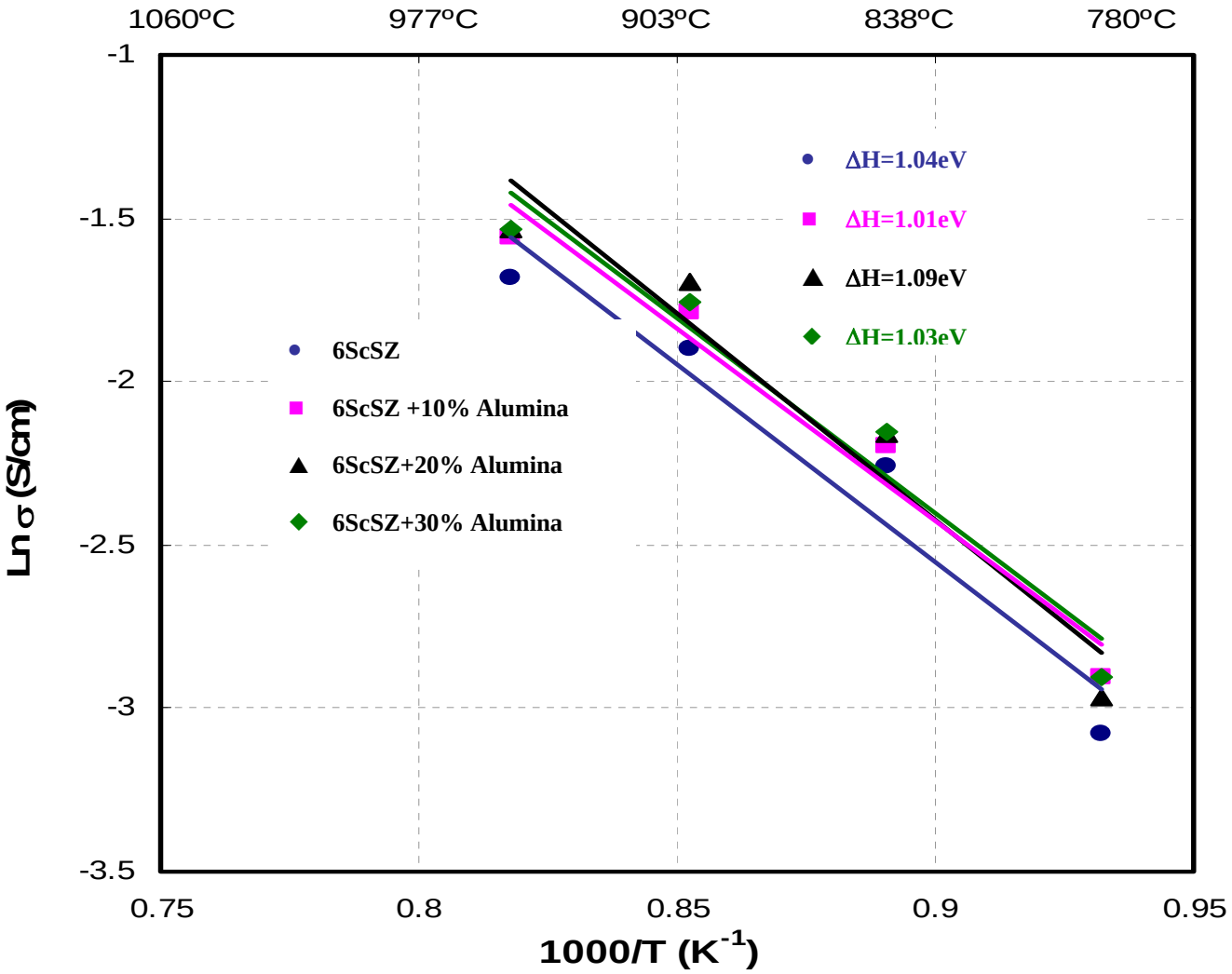

Figure 10. Arrhenius plots of all the 6ScSZ + Al_2O_3 composites.